Undergraduate Honors Thesis

The Role of Mitochondrial Biogenesis in Human Mesenchymal Stem Cell Differentiation and Acquisition of a Cardiac Phenotype

Author

Arun Ajmera

A thesis submitted to the Department of Biology, East Carolina University, in partial fulfillment of the requirements for BIOL 4995 Biology Honors Thesis.

Advisors

Barbara J. Muller-Borer, PhD

Ethan J. Anderson, PhD

Submitted to

Susan B. McRae, PhD

Department of Biology

East Carolina University

May 1, 2013

Biology Honors Thesis

The Role of Mitochondrial Biogenesis in Human Mesenchymal Stem Cell Differentiation and Acquisition of a Cardiac Phenotype

Arun Ajmera

Title

The Role of Mitochondrial Biogenesis in Human Mesenchymal Stem Cell Differentiation and Acquisition of a Cardiac Phenotype

Author

Arun Ajmera

Advisors

Barbara J. Muller-Borer, PhD

Ethan J. Anderson, PhD

Submitted to

Susan B. McRae, PhD

Department of Biology

East Carolina University

May 1, 2013

I hereby declare I am the sole author of this thesis. It is the result of my own work in partial collaboration with the Muller-Borer and Anderson laboratory. This thesis has not been submitted elsewhere for another degree.

Signed: Date

Arun Ajmera May 1st, 2013

Arun Ajmera

Dedication

I dedicate this thesis to my family:

To my father and mother, Shiv and Rajni Ajmera, for their constant love and support.

To my brother, Ajay Ajmera, for always being himself.

Epigraph

"I propose to tell you the secret of life…Though a little one, the master-word looms large in meaning. It is the open sesame to every portal, the great equalizer in the world, the true philosopher's stone, which transmutes all the base metal of humanity into gold. The stupid man among you it will make bright, the bright man brilliant, and the brilliant student steady. With the magic word all things are possible, and without it all study is vanity and vexation…

And the master-word is **Work**!"

Dr. William Osler

First Professor of Medicine

Johns Hopkins Hospital and Medical School

Acknowledgments

I would first like to thank Dr. Barbara J. Muller-Borer for being my mentor and being the first person to introduce me to research and its applications. I am grateful for all of her advice and guidance through this process; her instruction contributed to my understanding of stem cells. If not for her tolerance and patience, this thesis would not have been possible.

I would also like to thank Dr. Ethan J. Anderson for being my other mentor and instilling in me a love for research. His constant feedback and advice from the beginning of this project pushed this venture to a completed product. His involvement and persistence was crucial to this written accomplishment and my understanding of mitochondrial biogenesis.

Next, I would like to thank all the members of the Muller-Borer laboratory especially Payal Pradhan and Maria Collins. I am thankful to Payal for her early contributions to this project and for instructing me in basic lab protocols. I am thankful to Maria for teaching me many of the protocols and basics of data analysis needed to complete this thesis.

I would like to thank all members of the Anderson laboratory for their assistance and use of the Oroboros O_2K Oxygraph system, all members of Dr. Mary J. Thomassen's laboratory for their assistance and use of the PCR thermocycler, and Wenhuan Jiang from Dr. Xin-Hua Hu's laboratory for his assistance in image analysis and 3D reconstruction.

I am grateful to ECU's Department of Biology and Honors College for their support during my undergraduate tenure and during the completion of this thesis.

This project was funded by the Murray and Sydell Foundation, the Tulane Center for Gene Therapy through a grant from NCRR of the NIH (Grant # P40RR017447), the NIH grant HL098780, and the ECU Undergraduate Research and Creativity Award grant.

The Role of Mitochondrial Biogenesis in Human Mesenchymal Stem Cell Differentiation and Acquisition of a Cardiac Phenotype

Arun Ajmera

Department of Biology, East Carolina University, Greenville, NC 27858

ABSTRACT - **Introduction:** With an increased understanding of myocardial infarction, human mesenchymal stem cell (hMSC) transplantation therapies have shown promising results as a possible treatment for heart failure. However, little is known about mitochondrial biogenesis for hMSCs transplanted to a cardiac microenvironment, though mitochondria are vital to cell energy production, cellular differentiation, and cell death. The purpose of this study was to investigate the role of mitochondrial biogenesis in adult hMSC differentiation and acquisition of a cardiac phenotype. Based on recent experimental evidence, we hypothesized that mitochondrial activity would be enhanced when hMSC differentiation was directed towards a cardiac-like fate.

Methods: Two models to direct hMSC differentiation to a cardiac-like phenotype were evaluated. In Model # 1, hMSCs were co-cultured with neonatal rat cardiomyocytes for 48 hours. In Model # 2, hMSCs were treated with a combination of 3 growth factors (GF): insulin-like growth factor-1 (IGF-1), fibroblast growth factor-2 (FGF-2), and bone morphogenetic protein-2 (BMP-2) for 48 hours and 2.5 weeks. For both models qRT-PCR was performed on Mitochondrial Transcription Factor B1(TFB1M), Ubiquinol-Cytochrome C Reductase Core Protein 1(UQCRC1), Nuclear Respiratory Factor 1 (NRF-1), and Myocyte-specific Enhancer Factor 2C (MEF2C). In GF treated hMSCs, protein expression of

N-cadherin and mitochondrial Electron Transport Chain (ETC) complexes II, III, IV and V were evaluated, and mitochondrial O_2 consumption was assessed.

Results: Co-cultured hMSCs showed increased mitochondrial and cardiac specific gene expression when compared to control for TFB1M, UQCRC1, and MEF2C ($p \leq 0.05$). GF treated hMSCs showed increased mitochondrial gene expression of TFB1M ($p < 0.05$), increased O_2 consumption, and increased protein expression of mitochondrial ETC complex II and N-cadherin. No significant differences in cardiac specific gene expression were observed in GF treated hMSCs.

Conclusions: Both Models # 1 and # 2 exhibited various levels of increased mitochondrial biogenesis. Results from Model # 1 hMSCs suggest increased mitochondrial gene expression in early co-cultures, specifically Complex III, may play a role in early hMSC differentiation into a cardiac-like phenotype. Results of Model # 2 hMSCs suggest enhanced mitochondrial biogenesis with GF treatment and increased culture time may lead to improved hMSC survival and proliferation to enhance cell transplantation therapies.

Table of Contents

Table of Contents (continued)

List of Tables

List of Figures

List of Figures (continued)

List of Abbreviations

hMSC	human mesenchymal stem cell	MT-CO1	Mitochondrially encoded Cytochrome c oxidase I
GF	growth factor	NRF-1	Nuclear Respiratory Factor 1
IGF-1	insulin-like growth factor-1	TFB1M	Mitochondrial Transcription Factor B1
FGF-2	fibroblast growth factor-2	UCP3	Mitochondrial Uncoupling Protein 3
BMP-2	bone morphogenetic protein-2	UQCRC1	Ubiquinol-cytochrome c reductase core protein 1
ETC	Electron Transport Chain	FACS	Fluorescence Activated Cell Sorting
qRT-PCR	quantitative Real Time Polymerase Chain Reaction	EGTA	Ethylene Glycol Tetraacetic Acid
FBS	Fetal Bovine Serum	HEPES	N-2-hydroxyethylpiperazine-N-ethanesulfonic acid
DMEM	Dulbecco's Modified Eagle Medium	BSA	Bovine Serum Albumin
BNP	Brain Natriuretic Peptide	PBS	Phosphate Buffered Saline
CAMTA1	Calmodulin-binding transcription activator 1	SEM	Standard Error of the Mean
Cx43	Connexin 43	TBS	Tris-buffered saline
MEF2C	Myocyte-specific enhancer factor 2C	LDS	Lithium Dodecyl Sulfate
MYOCD	Myocardin	DDT	Dithothreitol
MFN2	Mitofusin-2	HRP	horseradish peroxidase

I. INTRODUCTION

Due to an increased understanding of myocardial infarction (MI) and development of congestive heart failure, stem cell transplantation therapies are being pursued as a therapeutic alternative to organ transplantation. Specifically, human mesenchymal stem cells (hMSCs) are a component of new cardiovascular cell based therapies. HMSCs are bone marrow derived pluripotent stem cells that proliferate and differentiate into a variety of specialized tissues including liver, neurons, fat, tendons, and muscle; possess immunomodulatory properties; and involve no ethical or immunological issues (Fukuhara et al. 1470-1480; Xu et al. 2658-2665; Labovsky et al. 93-101). HMSCs have also been demonstrated to differentiate into "cardiac-like cells" when placed *in vivo* and *in vitro* cardiac microenvironments (Kubo et al. 26-32; Labovsky et al. 93-101; Xu et al. 2658-2665; Fukuhara et al. 1470-1480; Muller-Borer et al. e38454). Yet, when transplanted, the precise mechanisms of stem cell survival, engraftment, and differentiation are not well understood (Pittenger and Martin 9-20). Due to this lack of understanding and hMSC's differentiation potential into many cell types, complications may occur during cell transplantation for cardiac therapy (Breitbach et al. 1362-1369; Li et al. 295-303; Labovsky et al. 93-101). Thus, elucidation of the factors that direct hMSC differentiation to a cardiac-like phenotype may improve therapeutic efficiency.

Differentiating hMSCs in co-culture models with neonatal rat cardiomyocytes is an accepted method to study hMSC cardiac-like differentiation (Labovsky et al. 93-101; Fukuhara et al. 1470-1480; Xu et al. 2658-2665; Li et al. 295-303). In co-culture, hMSCs exhibit cardiomyocyte like properties through cell-cell communication including the expression of cardiac specific genes and proteins along with Ca^{2+} excitation-contraction coupling (Muller-Borer et al. e38454). In this model, several signaling pathways including

Ca^{2+} dependent pathways have been studied and proposed as a signal to drive cardiac-like cell differentiation (Muller-Borer et al. e38454). Further studies are needed to elucidate other signaling pathways directing hMSC differentiation into cardiac like cells.

Another method for directing hMSC differentiation is through GF treatment of hMSCs in monoculture. This model has been shown to increase cardiac transcription factors and proteins similar to the co-culture model suggesting the GF treated hMSC model's intrinsic ability to differentiate into cardiac-like cells (Hahn et al. 933-943). When treated with a combination of GFs, hMSCs show increased survival in cardiac transplantation and improved therapeutic efficiency at sites with myocardial infarctions (Hahn et al. 933-943). Gap junction mediated cell-cell signaling and other signaling pathways that may direct GF treated hMSCs are under investigation. An understanding of the hMSC differentiation signaling pathway is critical for improved stem cell differentiation and therapy.

A possible signaling pathway involved in hMSC differentiation towards a cardiac-like phenotype is the mitochondrial biogenesis pathway. The role of mitochondrial biogenesis and bioenergetic function in adult stem cells currently remains largely unexplored, even though mitochondria are important in cell energy production, cell signaling, cellular differentiation, cell growth, and cell death (Duchen 365-451; Cho et al. 1472-1478; Facucho-Oliveira et al. 4025-4034; Piccoli et al. 26467-26476; Chung et al. S60-7). Improper functioning of this unique organelle has led to many mitochondrial maladies that have been linked to a wide range of disorders, including diabetes, cardiovascular disease, and cancer (Lonergan, Bavister, and Brenner 289-296; Duchen 365-451; Nesti et al. 165-171). Recently, the concept of mitochondrial biogenesis has been emerging as a concept critical to hMSC differentiation into various cell types and other advanced lineages (Pietila et al. 435-445; Nesti et al. 165-

171; Pietila et al. 575-588; Chen et al. 960-968). Thus, the goal of this study is to improve our basic understanding of stem cell differentiation in cardiac tissue regeneration and repair by investigating the role of mitochondrial biogenesis in adult hMSC differentiation and acquisition of a cardiac phenotype in a simulated cardiac co-culture microenvironment and in a growth factor treated monoculture model. Based on recent experimental evidence and new genomic data, it was hypothesized that mitochondrial activity and biogenesis would be enhanced in hMSCs when placed in a microenvironment to direct cardiomyocyte differentiation.

II. MATERIALS AND METHODS

Two cell culture models reported to direct hMSCs towards a cardiac like phenotype were used in this investigation. In Model # 1, hMSCs were co-cultured with neonatal rat cardiac myocytes or grown in monoculture as a control for 48 hours. After 48 hours, the following experiments were performed in control and co-cultured hMSCs:

- CD 90 magnetic bead separation to isolate hMSCs
- qRT-PCR to evaluate cardiac and mitochondrial gene expression

Study limitations prevented further analysis in Model # 1; therefore, Model # 2 (GF treated hMSCs) was studied.

In Model # 2, hMSCs were treated with a combination of GFs and evaluated at 48 hours and 2.5 weeks. For hMSCs treated with GFs for 48 hours, qRT-PCR was performed to evaluate differences in mitochondrial gene expression between control and GF treated hMSCs. For hMSCs treated with GFs for 2.5 weeks, the following experiments were completed:

- qRT-PCR to evaluate cardiac and mitochondrial gene expression
- Western blot analysis to evaluate cardiac and mitochondrial protein expression
- O_2 consumption to evaluate mitochondrial content and oxidative capacity
- 2D/3D Imaging with 3D reconstruction analysis to evaluate mitochondrial localization and morphology

A. Cell Culture and Separation

Frozen vials of dsRed hMSCs (from healthy donors transduced with dsRed fluorescent protein) were purchased from the Tulane Center for the Preparation and Distribution of Adult Stem Cells and Tulane Center of Gene Therapy. Prior to shipping, the hMSCs were transduced with the lentiviral vector WPT-EF1 short-DsRed2-mito pseudotyped with a Vesicular stomatitis virus G protein envelope in the presence of polybrene. Fluorescence Activated Cell Sorting (FACS) isolation was used to positively select for hMSCs with dsRed fluorescent protein. The vector encodes a dsRed fluorophore that stably targets subunit VIII of cytochrome c oxidase (mitochondrial ETC complex IV) under the control of the EF1-short promoter.

1. *Model # 1 – hMSC co-culture with cardiomyocytes and separation*

    a. Cardiomyocyte Isolation and Culture

    Cardiomyocyte primary cultures were established in order to make a myocardial microenvironment for the hMSCs. Neonatal rat cardiomyocytes were isolated from the hearts of 1 day old Sprague Dawley rats using a Worthington Neonatal Cardiomyocyte Isolation System (Worthington Biochemical Corp., Lakewood, NJ) in accordance with accepted guidelines for the care and treatment of experimental animals at East Carolina University's Brody School of Medicine and the National Institutes of Health. The cardiomyocytes were grown for 5 days in Richter (Irvine Scientific, Santa Ana, CA) medium supplemented with 10% Fetal Bovine Serum (FBS) before co-culturing with hMSCs.

b. Model # 1 - Co-cultured hMSCs

HMSCs were co-cultured with neonatal rat cardiomyocytes in a 1:10 ratio (hMSCs to cardiomyocytes) in flasks and grown in a cell culture incubator (5% CO_2 and 37°C) with full media (16.5% FBS in Dulbecco's Modified Eagle Medium [DMEM]). The control hMSCs were grown in monocultures under identical conditions, i.e. incubator environment, full media, and length of time in culture.

c. CD 90 Magnetic bead separation

After 48 hours of co-culture, the hMSCs were separated from the cardiac myocytes using a CD 90 magnetic bead separation procedure following the vendor's protocol (DYNAL - Dynabeads® Pan Mouse IgG from Invitrogen). CD 90, a stem cell marker located on the cell membrane surface, is expressed on hMSCs. Magnetically labeled CD 90 Microbeads were added to a cell suspension containing the co-cultured hMSCs and cardiomyocytes and a cell suspension containing the control hMSCs (indirect technique). In both cell suspensions, the CD 90 antibody on the magnetic microbeads binded to the respective CD 90 stem cell marker on the hMSC membrane surface. The suspensions were passed through a magnetic separation column, where a magnet isolated the labeled hMSCs leaving any unlabeled cells including co-cultured cardiomyocytes and unlabeled hMSCs to elute through the column and be collected as eluate. The isolated hMSCs were collected and harvested to evaluate cardiac and mitochondrial gene expression with qRT-PCR. The control hMSCs were treated

to the same separation protocol. RLT buffer was added to harvested hMSCs to isolate and preserve the RNA for qRT-PCR.

2. Model # 2 – GF Treated hMSCs

In Model # 2, hMSCs were plated in flasks and grown in a cell culture incubator (5% CO_2 and 37°C) with full media and antibiotics (16.5% FBS and 1% Penicillin/Streptomycin in DMEM) along with a combination of 3 GFs. The 3 GFs used in the experiment were IGF-1 (2 ng/mL), FGF-2 (50 ng/mL), and BMP-2 (10 ng/mL). GFs were added to hMSCs during each media change every 3-4 days (for hMSCs treated with GFs for 2.5 weeks). The control hMSCs were grown under identical conditions as the GF treated hMSCs but without GFs. After 48 hours or 2.5 weeks in culture, the hMSCs were harvested. TrypLE express recombinant trypsin (Gibco 12605) was added to flasks containing hMSCs and incubated for 5 minutes at 37°C in order to lift cells off the flask. Full media with FBS was added after 5 minutes to stop the trypsin enzyme activity. Cells suspended in full media were collected in 50 mL conical tubes and spun in a centrifuge at 1500 RPM for 5 minutes in order to precipitate cell pellets. The pellets were washed with sterile Phosphate Buffered Solution (PBS) and re-suspended in fresh media for hMSCs to be counted on a hemacytometer. RLT buffer was added to isolated hMSCs to preserve the RNA for qRT-PCR. For western blot analysis, cell pellets were resuspended in Tris-buffered saline (TBS) for washing. Afterwards, lysis buffer was added for western blot analysis.

B. Cardiac and Mitochondrial Gene Expression with qRT-PCR

1. Extraction and Quantification of RNA

All hMSCs harvested in Model # 1 (the control hMSCs, the isolated hMSCs, and the cardiomyocytes), all hMSCs harvested in Model # 2 after 48 hours of GF treatment (control and GF treated), and 5.0×10^6 hMSCs harvested from each group in Model # 2 after 2.5 weeks of GF treatment (control and GF treated) were lysed by adding RLT buffer from a RNeasy mini kit (Qiagen Cat. # 74104) for RNA isolation and preservation in order to evaluate gene expression via qRT-PCR. After preserving the RNA with RLT buffer, ethanol along with RW1 and RPE buffer from the RNeasy mini kit was used to extract RNA from the lysed cell contents. Afterwards, the extracted RNA was taken to the NanoDrop 1000 Spectrophotometer to measure RNA yield.

2. Synthesis of cDNA and qRT-PCR

RT master mix (High Capacity cDNA Reverse Transcription Kit – Invitrogen part # 4368814) was added to quantified RNA and placed in a ABI 7300 thermocycler to synthesize cDNA. The ABI temperature and time conditions for synthesizing cDNA are identified in Table 1A as a total of 4 steps. In Step 1, the primers used in cDNA synthesis were extended at 25°C for 10 minutes. In Steps 2 and 3, cDNA was synthesized at 37°C. Afterwards, cDNA synthesis was completed by terminating the reaction at 85°C in Step 4.

The synthesized cDNA was added to 96 well plates with TaqMan Master Mix and TaqMan gene probes to conduct qRT-PCR. The 96 well plates were placed in the

thermocycler again to synthesize copies of RNA selected by the gene probes. The ABI temperature and time conditions for qRT-PCR are identified in Table 1B. The first two steps were used to initiate reverse transcription. Afterwards, Steps 3 and 4 were repeated 40 times sequentially. Step 3 was used for denaturing cDNA, and Step 4 was used for annealing and extending the cDNA strands. The ct values were recorded and used to evaluate gene expression as fold difference in the monoculture control vs. the co-cultured hMSCs in Model # 1 and in the control vs. the GF treated hMSCs in Model # 2.

In Models # 1 and # 2, qRT-PCR was conducted to evaluate cardiac and mitochondrial gene expression. The cardiac genes tested for gene expression have been shown to be expressed during cardiac differentiation and in cardiomyocytes. To evaluate mitochondrial gene expression, potentially significant mitochondrial biogenesis genes were identified from querying the GEO Microarray Database (NCBI-GEO data base accession number GSE32171) obtained by the Muller-Borer laboratory for the co-culture model (Muller-Borer et al. e38454). Shown below in Table 2 is a description of the cardiac and mitochondrial genes used as TaqMan gene probes for qRT-PCR in Models # 1 and # 2.

Table 1: Temperature and Time Conditions in ABI 7300 thermocycler

Table 1A: ABI Thermocycler Conditions for Synthesizing cDNA				
	Step 1	**Step 2**	**Step 3**	**Step 4**
Temperature (°C)	25	37	37	85
Time (min.)	10	60	60	5

Table 1B: ABI Thermocycler Conditions for qRT-PCR				
	Step 1	**Step 2**	**Step 3**	**Step 4**
Cycles			**40 Cycles – Step 3 ->Step 4 (Repeat)**	
Temperature (°C)	50	95	95	60
Time (min.)	2	10	0.25	1

Table 2: Summary of Cardiac and Mitochondrial Genes

Gene Type	Abbreviation	Full name	Description
Cardiac Genes	BNP	Brain Natriuretic Peptide	Natriuretic peptide synthesized within the ventricles and encodes a secreted protein that functions as a cardiac hormone
	CAMTA1	Calmodulin-binding transcription activator 1	Expressed in brain tissue, heart, and kidney; interacts with and possibly regulates calmodulin, a universal calcium sensor; and functions as a transcriptional activator
	Cx43	Connexin 43	Gap junction found in ventricular myocardium and is also known as the main cardiac connexin
	MEF2C	Myocyte-specific enhancer factor 2C	Transcription factor found at all stages of cardiac development and is up regulated with cell hypertrophy
	MYOCD	Myocardin	Regulates cardiac and smooth muscle gene expression
Mitochondrial Genes*****	MFN2	Mitofusin-2	Involved in mitochondrial fusion and contributes to maintenance of mitochondrial viability in cells
	MT-CO1	Mitochondrially encoded Cytochrome c oxidase I	Encodes protein from mitochondrial DNA to form an ETC complex IV subunit
	NRF-1	Nuclear Respiratory Factor 1	Functions as a transcription factor for activating metabolic genes, and is involved in early stages of mitochondrial biogenesis in muscle development
	TFB1M	Mitochondrial Transcription Factor B1	Encodes a mitochondrial transcription factor that is suggested to activate key genes in mitochondrial biogenesis
	UCP3	Mitochondrial Uncoupling Protein 3	Reduces the mitochondrial membrane potential as a proton leak, and is involved in negating oxidative stress
	UQCRC1	Ubiquinol-cytochrome c reductase core protein 1	Encodes protein from nuclear DNA to form an ETC complex III subunit

*****: Mitochondrial genes in Table 2 considered significant in the queried GEO Microarray Database

C. Western Blot Analysis in Model # 2

The lysis buffer added to cell pellets for western blot analysis was 0.5% of Triton X-100 and 0.1% of Protease Inhibitor Cocktail (Sigma P8340) in TBS (pH = 7.2). After vortexing and centrifuging, the cell lysate in the supernatant was obtained and the insoluble debris was discarded. Protein concentration from cell lysate was quantified via a standard curve analysis. Afterwards, protein samples were prepared in 1X NuPage lithium dodecyl sulfate (LDS) sample buffer and in the reducing agent 1X dithothreitol (DDT). Western blot analysis was performed by loading 60 ug of protein sample per well in a BioRad 4-12% Bis Tris gel. After running the gel with NuPage MOPS running buffer via electrophoresis (175 V for 55 minutes), the gel was transferred to a Nitrocellulose membrane (60 V for 1 hour and 15 minutes) with Towbins transfer buffer. Once transfer was complete, the membrane was blocked with 5% milk in TBS. Washes were completed between the additions of the primary and secondary antibody using 0.1 % Tween 20 in TBS. The following primary antibodies (diluted with 5 % milk in TBS) shown in Table 3 were added to the membrane after washing 3 times. After adding the primary antibodies to the membrane and washing again for 3 times, a secondary antibody tagged with horseradish peroxidase (HRP) from Invitrogen^{TM} was added. A chemiluminescent substrate was added to the membrane to detect HRP. The membrane was exposed to photographic film. The exposed film was developed by a film developer. The bands on the developed film underwent densitometric analysis to evaluate the relative amount of protein as a percent of the control.

Table 3: Summary of Primary and Secondary Antibodies for Western Blot Analysis

Primary Antibody	Secondary Antibody	Description
Mouse Anti-Human Connexin-43 Monoclonal Antibody	Goat Anti-Mouse	Used to determine protein expression of gap junction protein (the main cardiac connexin)
Mouse Anti-Human N-Cadherin	Goat Anti-Mouse	Used to determine protein expression of a cell adhesion transmembrane protein
Mouse Anti-Human Total OXPHOS Antibody	Goat Anti-Mouse	Used to determine protein expression of mitochondrial ETC Complexes I-V
Rabbit Anti-Human β-actin	Goat Anti-Rabbit	Used as a loading control for Western Blot analysis

D. O_2 Consumption Experiments in Model # 2

After harvesting control hMSCs and GF treated hMSCs from Model # 2 (2.5 weeks of GF treatment), O_2 consumption experiments were performed by using 1.5 million cells from each group. Control hMSCs and GF treated hMSCs were permeabilized by suspending with 4.5 µg/mL of digitonin in MiR05 and 1mM EGTA respiratory buffer for 5 minutes. Contents of MiR05 respiratory buffer are shown in Table 4. After 5 minutes, cells were centrifuged at 1000 RPM for 5 minutes. The supernatant was removed and the cell pellets were re-suspended in 2 mLs of fresh MiR05 and 1mM EGTA respiratory buffer without digitonin. The 2 mLs from each group were injected into separate sealed chambers of the Oroboros O_2K Oxygraph System. Equal amounts of O_2 were also injected into both chambers containing the permeabilized hMSCs. The total O_2 consumption and the O_2 consumption rates were measured with the addition of the following mitochondrial specific substrates and inhibitors shown in Table 5. A visual model showing where the mitochondrial specific substrates and inhibitors act upon is visible in Figure 1.

Table 4: Contents of MiR05 Respiratory Buffer

Name	Final Concentration
$MgCl_2 \cdot 6H_2O$	3mM
K-lactobionate	60mM
Taurine	20mM
KH_2PO_4	10mM
HEPES	20mM
Sucrose	110mM
BSA	1 gram/L

Table 5: Summary of Mitochondrial Substrates and Inhibitors

Name	Substrate or Inhibitor	Description
5mM Pyruvate / 2mM Malate	Complex I Substrates	Substrates form NADH. NADH donates electrons to fuel Complex I (NADH Dehydrogenase) to initiate O_2 consumption (state IV respiration)
5mM ADP	ATP Synthase Substrate / Energy Acceptor	Substrate binds to ATP Synthase and triggers O_2 consumption (state III respiration) by stimulating oxidative phosphorylation
5mM Succinate	Complex II Substrate	Substrate forms FADH. FADH donates electrons to fuel Complex II (Succinate Dehydrogenase)
1ug/mL Rotenone	Complex I Inhibitor	An insecticide and fish poison that blocks electron transport between Complex I and ubiquinone
1ug/mL Oligomycin	ATP Synthase Inhibitor	A macrolide antibiotic that blocks the proton channel of ATP Synthase

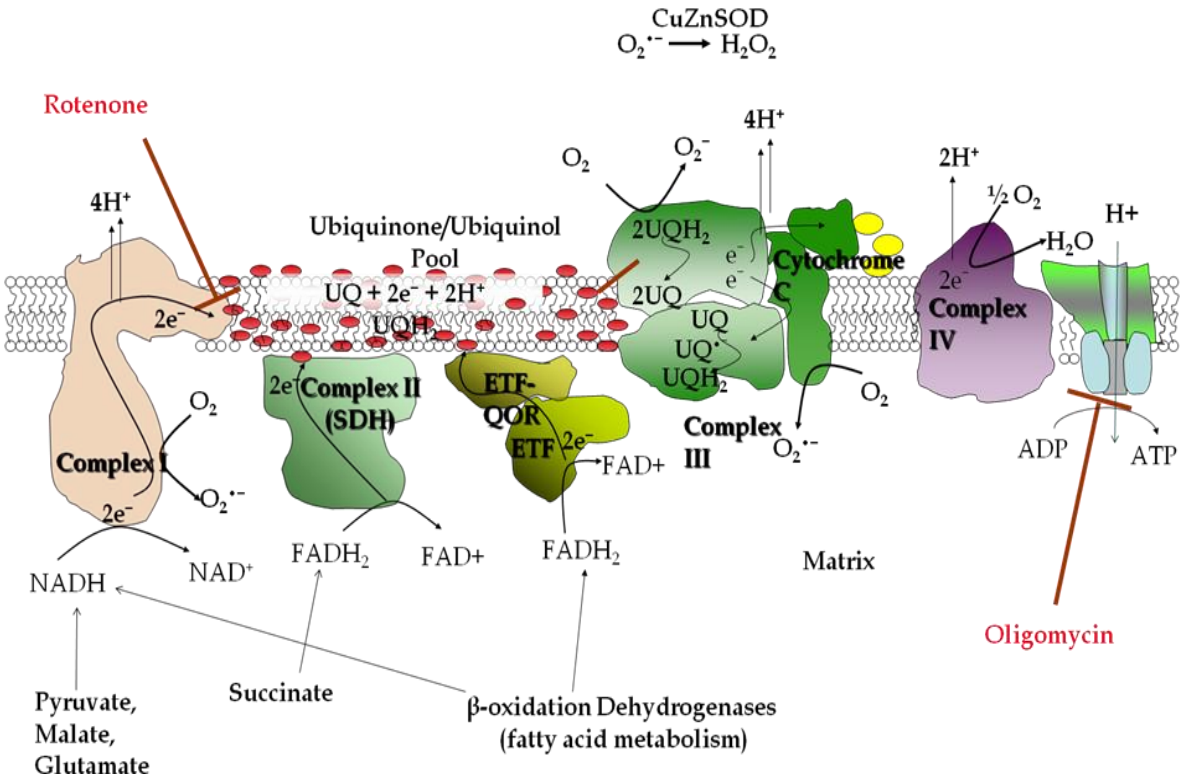

Figure 1: Electron Transport Chain (ETC) on the Inner Mitochondrial Membrane. Pyruvate, Malate, and Glutamate are Complex I substrates. Succinate is a Complex II substrate. Rotenone is a Complex I inhibitor. Oligomycin is an ATP Synthase inhibitor. Figure was provided by Dr. Anderson.

E. 2D and 3D Imaging with 3D Reconstruction in Model # 2

Two dimensional (2D) laser scanning confocal imaging was performed on GF treated and control hMSCs to determine mitochondrial localization. Three dimensional (3D) laser scanning confocal imaging with 3D reconstruction was also performed to evaluate changes in 3D cell morphology in GF treated vs. control hMSCs to quantitate 3D mitochondrial morphology.

1. 2D Imaging

DsRed hMSCs (both control and GF treated) were imaged on a confocal microscope (Zeiss LSM 510) in media containing 10% FBS without phenol for 2D imaging at different culture times. The hMSCs (both control and GF treated) were imaged after 4 days as an early culture time point and imaged after 11 days as a later culture time point to observe mitochondrial localization.

2. 3D Imaging

The dsRed hMSCs were grown with and without GFs for 2 weeks. Control and GF treated hMSCs were removed from flasks using TrypLE express recombinant trypsin and re-suspended in dye media. The cytosolic dye Calcein AM (494 nm excitation and 517 nm emission, 1 µM) and nuclear dye Syto61 (628 nm excitation and 645 nm emission, 1 µM) were added to control and GF treated hMSCs. Syto61 was used for labeling the nucleus. Calcein AM was used to label the cytoplasm. The fluorescent protein dsRed (545 nm excitation and 572 emission) was used to target the mitochondria. After incubation in both dyes for 15 minutes, hMSCs were washed with PBS and re-suspended in media containing 10% FBS without phenol before

imaging on the Olympus FV1000 confocal microscope. HMSCs were suspended between 2 glass coverslips and placed in a coverslip chamber to stabilize cell media and reduce cell motion. During 3D confocal imaging, 1 µm crossections were acquired and averaged 24 image slices during Z stack acquisition. Image alignment of crossection slices was completed using an algorithm developed in Dr. Hu's laboratory to minimize distortions in 3D reconstructions caused by potential cell motion (Ekpenyong et al. 73671J-73671J). Figure 2 shows 3D image segmentations of both control and GF treated hMSCs.

3. 3D Reconstruction

Imaging software developed in Dr. Hu's laboratory was used to align and create 3D reconstructions of the hMSCs (Ekpenyong et al. 73671J-73671J). Pixels from each confocal image slice were sorted on a histogram analysis according to fluorescent intensity into 4 groups: background, cytoplasm, mitochondria, and nucleus. After separation of pixels into their correct compartments, the confocal images were assembled by interpolation, forming a stl file format for 3D viewing. This computer generated 3D reconstruction minimized errors in the z axis interpolation (along with random and systematic error) by employing a z scan correction factor and image processing methods (Ekpenyong et al. 73671J-73671J). The computer generated 3D reconstructions were used to quantitate overall cell morphology and mitochondrial morphology.

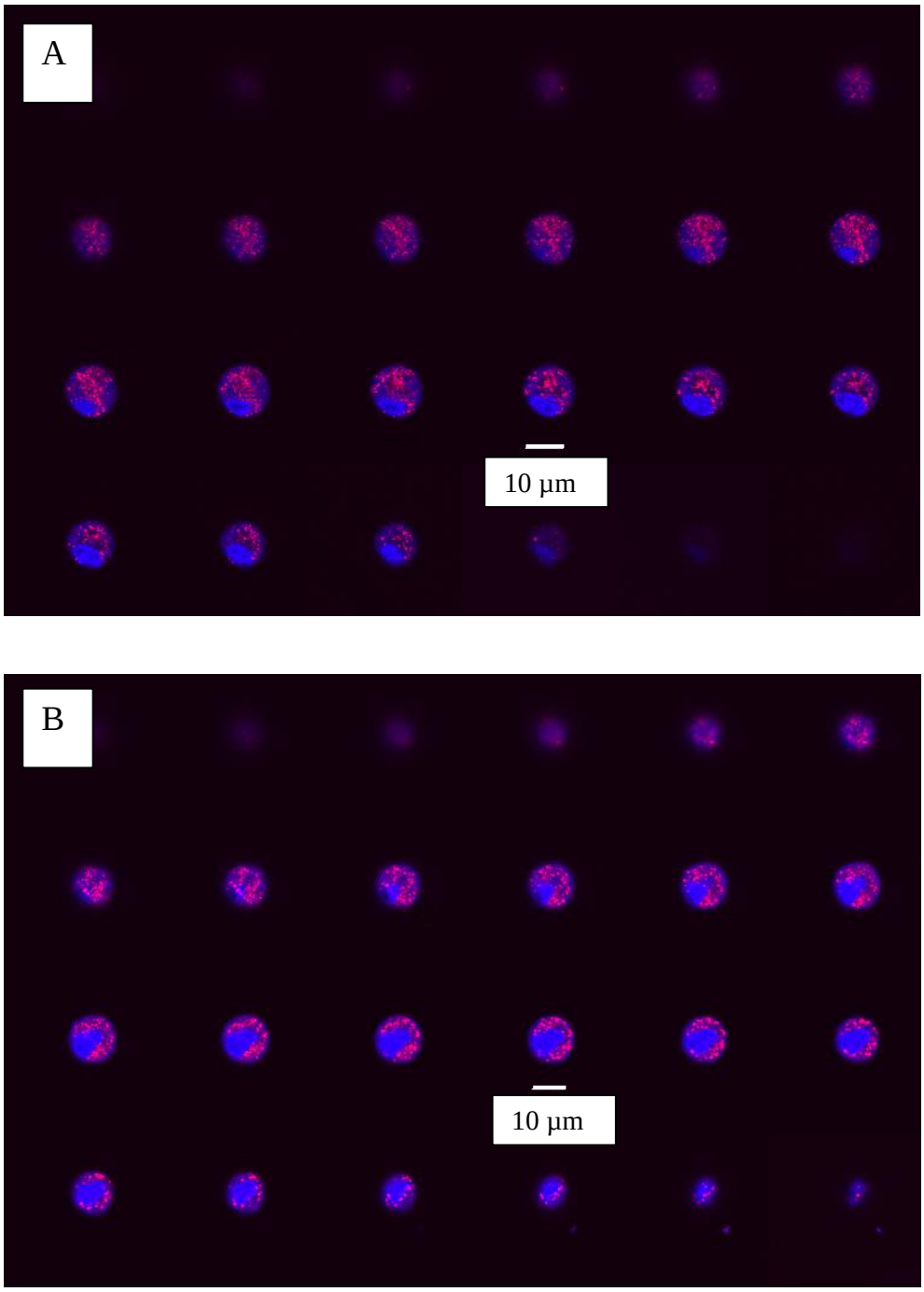

Figure 2: Segmentation of 3D Confocal Imaging in GF Treated hMSCs. A: A control hMSC with 24 crossection slices is shown in segmented (top to bottom) form where each crossection is 1 µm apart. Nucleus is shown in blue and mitochondria are shown in red. **B:** The same is shown for a GF treated hMSC in B.

III. RESULTS

A. Cardiac and Mitochondrial Gene Expression

1. Model # 1: Cardiomyocyte and hMSC Co-culture

Cardiac and mitochondrial gene expression was measured in hMSCs after 48 hours in co-culture. Figure 3 shows the results of qRT-PCR for cardiac gene expression. Figure 4 shows the results of qRT-PCR for mitochondrial gene expression. Results for all qRT-PCR co-cultured hMSC data are indicated as fold difference of control hMSCs. Error bars on figures represent the standard error of the mean (SEM).

A significant increase in MEF2C was measured in co-cultured hMSCs vs. control hMSCs ($p < 0.01$). Expression of the transcription factor CAMTA-1 showed a slight decrease in co-cultured hMSCs vs. control; however, the decrease was not statistically significant ($p = 0.09$). Other cardiac genes in Table 2 were not evaluated using qRT-PCR in this model.

Significant increases of mitochondrial gene expression were present in co-cultured hMSCs compared to control. A significant increase in TFB1M, a mitochondrial transcription factor, was measured in co-cultured hMSCs compared to control hMSCs ($p \leq 0.05$). A significant increase in the mitochondrial ETC complex III subunit, UQCRC1, was measured in co-cultured hMSCs compared to the control ($p < 0.05$). No significant differences in other mitochondrial genes evaluated in co-cultured hMSCs vs. control hMSCs were measured as shown in Figure 4.

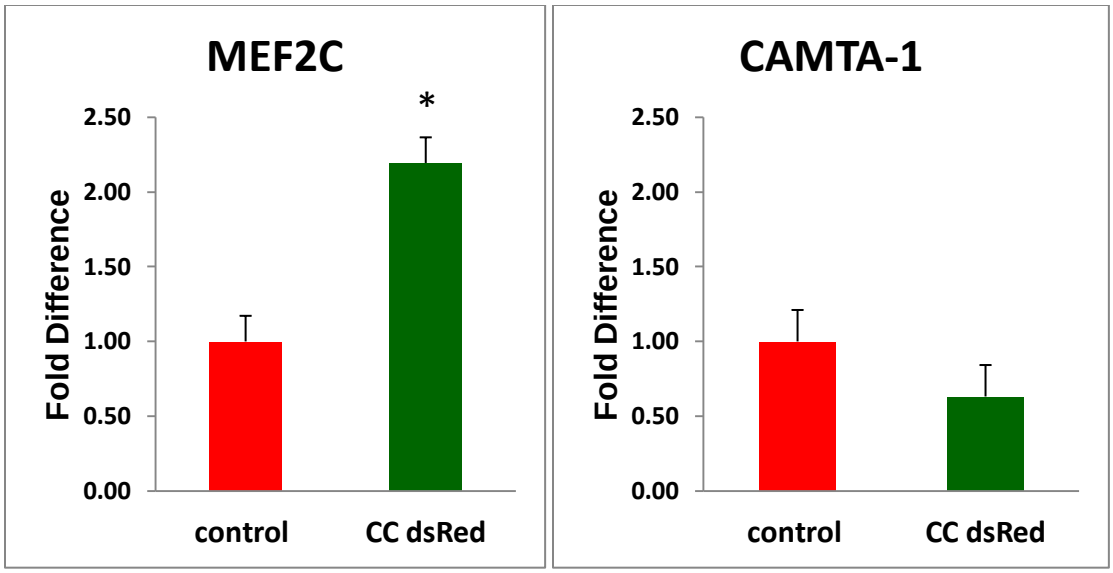

Figure 3: Cardiac Gene Expression in Co-culture model. MEF2C showed significantly increased expression in co-cultured hMSCs compared to control hMSCs ($p < 0.01$). CAMTA-1 showed decreased expression in co-cultured hMSCs compared to control hMSCs; however, this decrease was not statistically significant ($p = 0.09$). The bars show mean ± SEM ($n = 3$).

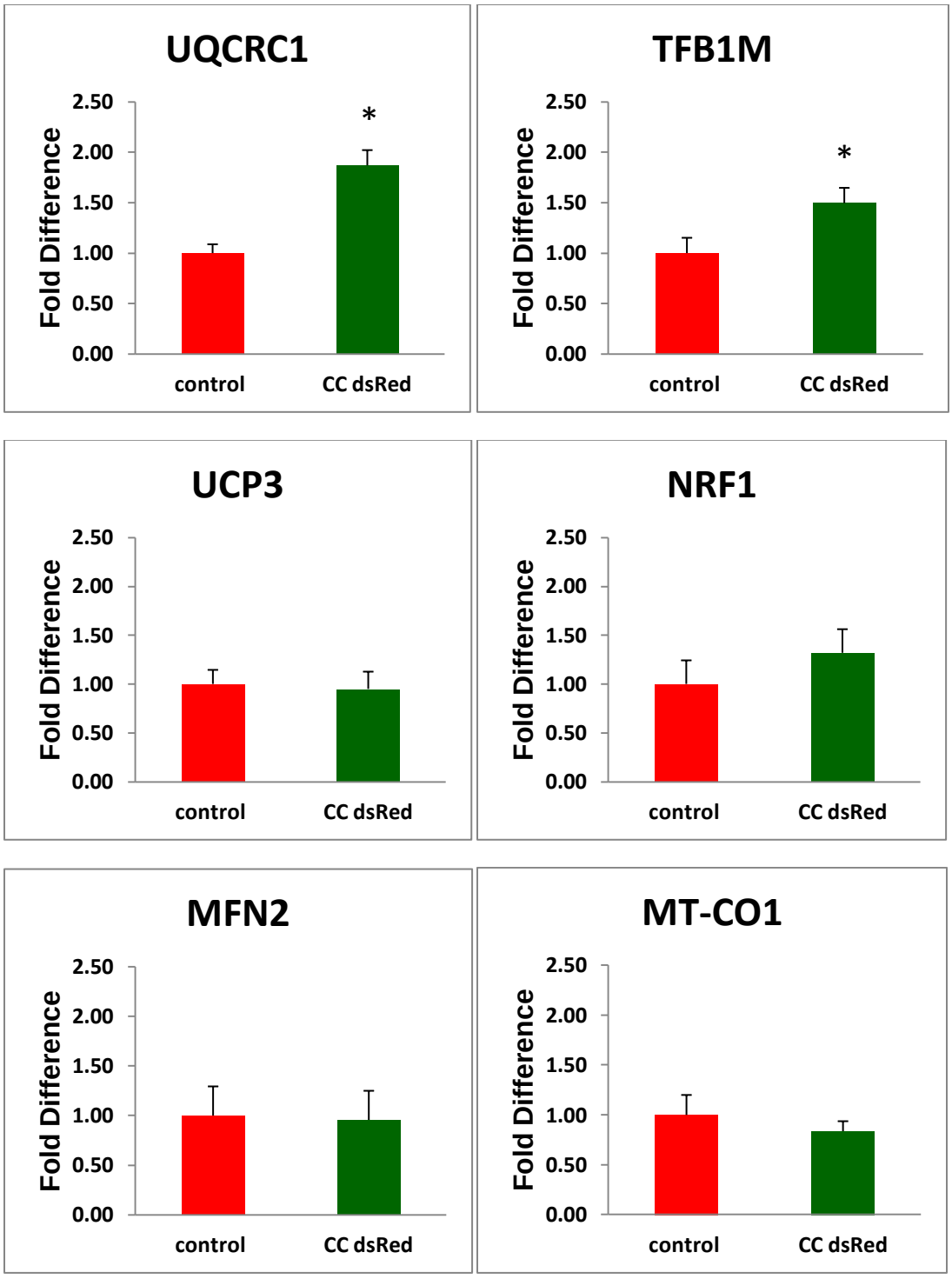

Figure 4: Mitochondrial Gene Expression in Co-culture model. UQCRC1 showed a significant increase of expression in co-cultured hMSCs compared to the control hMSCs ($p < 0.05$). TFB1M was significantly increased in co-cultured hMSCs compared to the control hMSCs ($p \leq 0.05$). NRF1, MFN2, UCP3, and MT-CO1 showed no significant difference in gene expression in co-cultured hMSCs compared to control hMSCs. The bars show mean ± SEM ($n = 3$).

2. Model # 2: GF Treated hMSC Monoculture

Mitochondrial gene expression was measured in hMSCs after 48 hours of GF treatment. Figure 5 shows these results for TFB1M, UQCRC1, and NRF-1. Results for all qRT-PCR in GF treated hMSC data are indicated as fold difference of control hMSCs. Error bars on figures represent SEM. No significant difference in gene expression for mitochondrial genes evaluated was measured in GF treated hMSCs (48 hours) vs. control hMSCs as shown in Figure 5 ($p > 0.05$).

Cardiac and mitochondrial gene expression was measured in hMSCs after 2.5 weeks of GF treatment. Figure 6 shows the results of qRT-PCR for cardiac gene expression. Figure 7 shows the results of qRT-PCR for mitochondrial gene expression. Overall, qRT-PCR showed high variability for hMSCs in the 2.5 week GF treated model.

No significant difference in gene expression for cardiac genes evaluated was measured in GF treated hMSCs (2.5 weeks) vs. control hMSCs as shown in Figure 6. All cardiac genes in Table 2 were evaluated via qRT-PCR in this model.

For mitochondrial gene expression, a significant increase in TFB1M was measured in GF treated hMSCs (2.5 weeks) compared to control hMSCs ($p < 0.05$). There was no significant difference in expression of the mitochondrial ETC complex III subunit, UQCRC1, in GF treated hMSCs (2.5 weeks) compared to control hMSCs as shown in Figure 7. No significant differences in the mitochondrial genes MFN2, MT-CO1, NRF-1, and UCP3 were measured in GF treated hMSCs (2.5 weeks) and control hMSCs (data not shown).

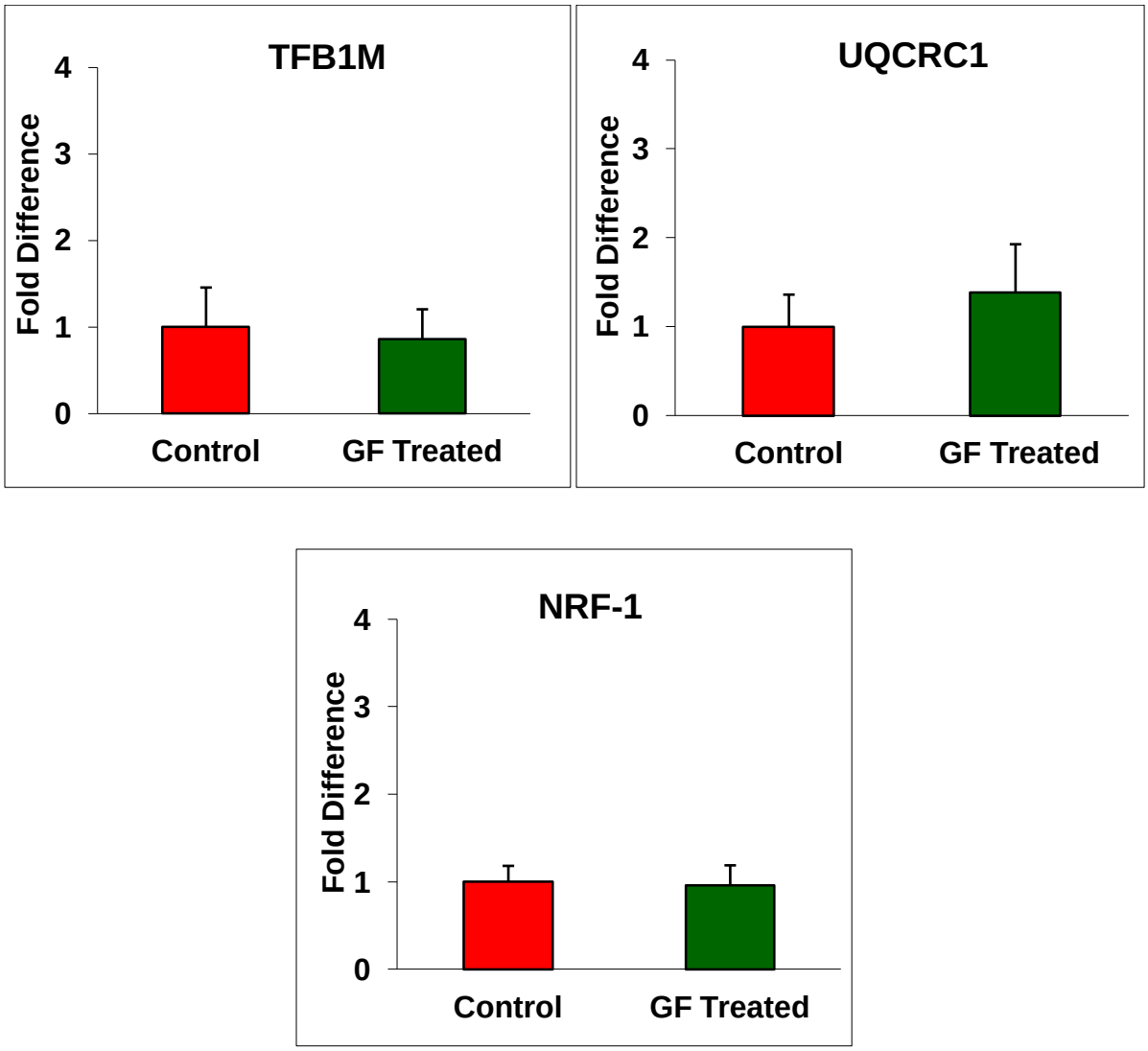

Figure 5: Mitochondrial Gene Expression in 48 hour GF Treated Model. No significant difference in gene expression for TFB1M, UQCRC1, and NRF-1 were measured in GF treated hMSCs (48 hours) compared to control hMSCs ($p > 0.05$). Results are represented as $n = 3$. The bars show mean ± SEM.

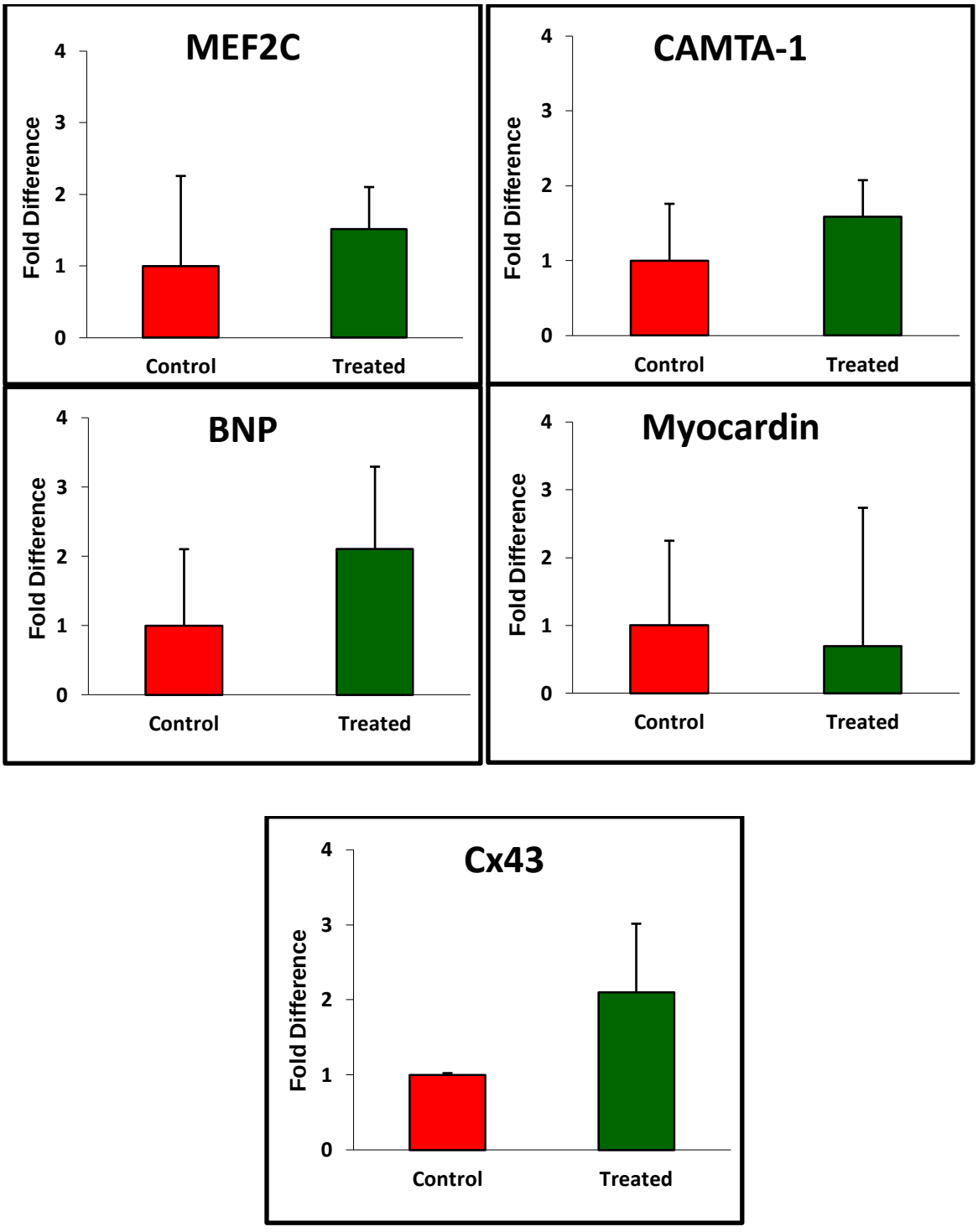

Figure 6: Cardiac Gene Expression in 2.5 Week GF Treated Model. There was no significant difference of cardiac gene expression in the GF treated vs. control hMSCs. For MEF2C, CAMTA-1, BNP, and Myocardin, results are represented as n = 3. For Cx43, results are represented as n = 2. The bars show mean ± SEM.

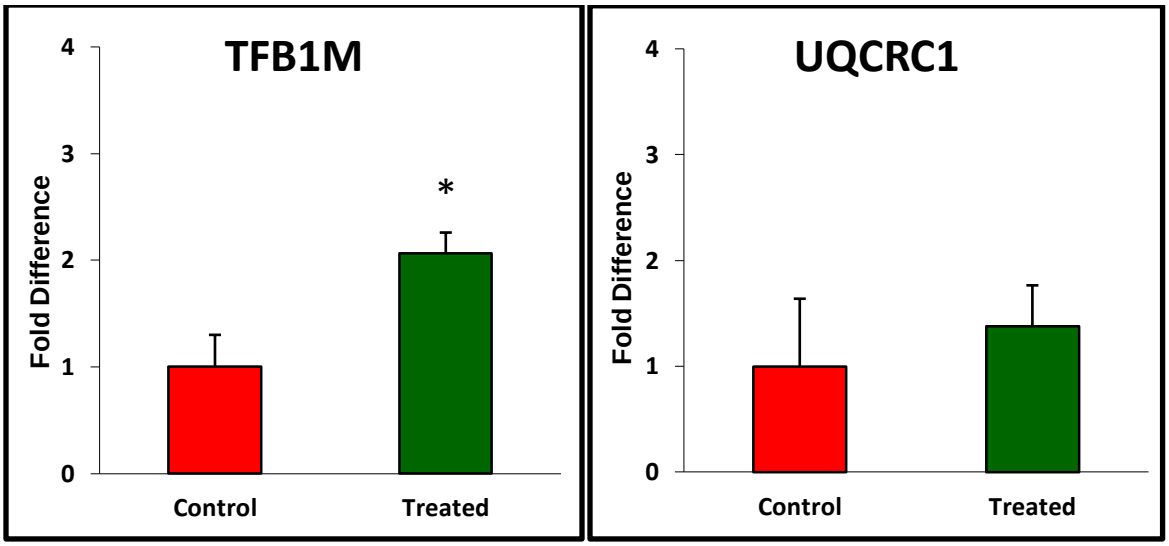

Figure 7: Mitochondrial Gene Expression in 2.5 Week GF Treated Model. TFB1M was significantly increased in GF treated hMSCs compared to control hMSCs at 2.5 weeks ($p < 0.05$). There was no significant change of UQCRC1 expression in GF treated hMSCs compared to control hMSCs. The bars show mean ± SEM (n = 3).

B. Western Blot Analysis

Results of the western blot analysis for mitochondrial ETC complex II, III, IV, V, Cx 43, and N-Cadherin are represented below in Figure 8 and Figure 9. Figure 8 illustrates the protein bands from 2.5 week GF treated hMSCs and control hMSCs. Protein loading control was confirmed for all bands in Figure 8 via β-actin or Ponceau S staining. Compiled data from 4 experiments is shown in Figure 9.

Mitochondrial ETC complex II showed increased protein expression in GF treated hMSCs compared control hMSCs as shown in Figure 8, and averaged a twofold increase of protein expression with 4 replicate experiments as shown in Figure 9. N-Cadherin showed increased protein expression in GF treated hMSCs compared control hMSCs as shown in Figure 8, and averaged a fourfold increase of protein expression with 4 replicate experiments as shown in Figure 9. No difference in mitochondrial ETC complex III protein expression in Figure 8 and Figure 9 resembles the qRT-PCR results for UQCRC1, the mitochondrial ETC complex III subunit.

No significant differences in expression of the cardiac gap junction, Cx 43, and the mitochondrial ETC complex V were measured as shown in Figure 8 and Figure 9. Mitochondrial ETC complex I protein expression was also evaluated; however, bands were not visible at the completion of western blots suggesting a faulty antibody for complex I or lack of complex I expression in both hMSC groups compared to other mitochondrial ETC complex proteins.

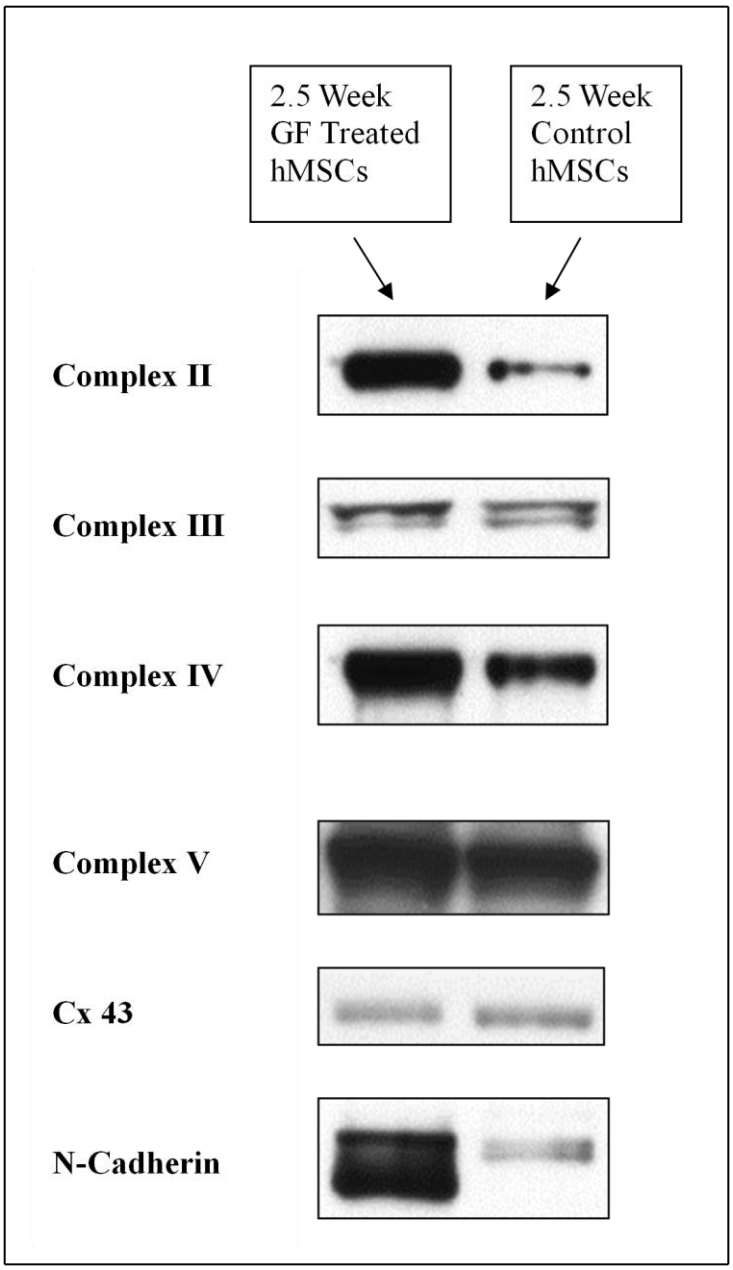

Figure 8: **Cardiac and Mitochondrial Protein Expression from 2.5 week GF treated hMSCs.** Complex II and IV showed increase of expression with 2.5 weeks of GF treatment. Complexes III and V showed no difference in control and GF treated hMSCs. For cardiac protein expression, Cx 43 gap junction showed no observable difference in GF treated hMSCs compared to control. N-Cadherin, a cardiac tight junction, showed a clear increase of expression with 2.5 weeks of GF treatment. Results shown are representative data. Equal protein loading for all data shown above was confirmed via β-actin or Ponceau S staining.

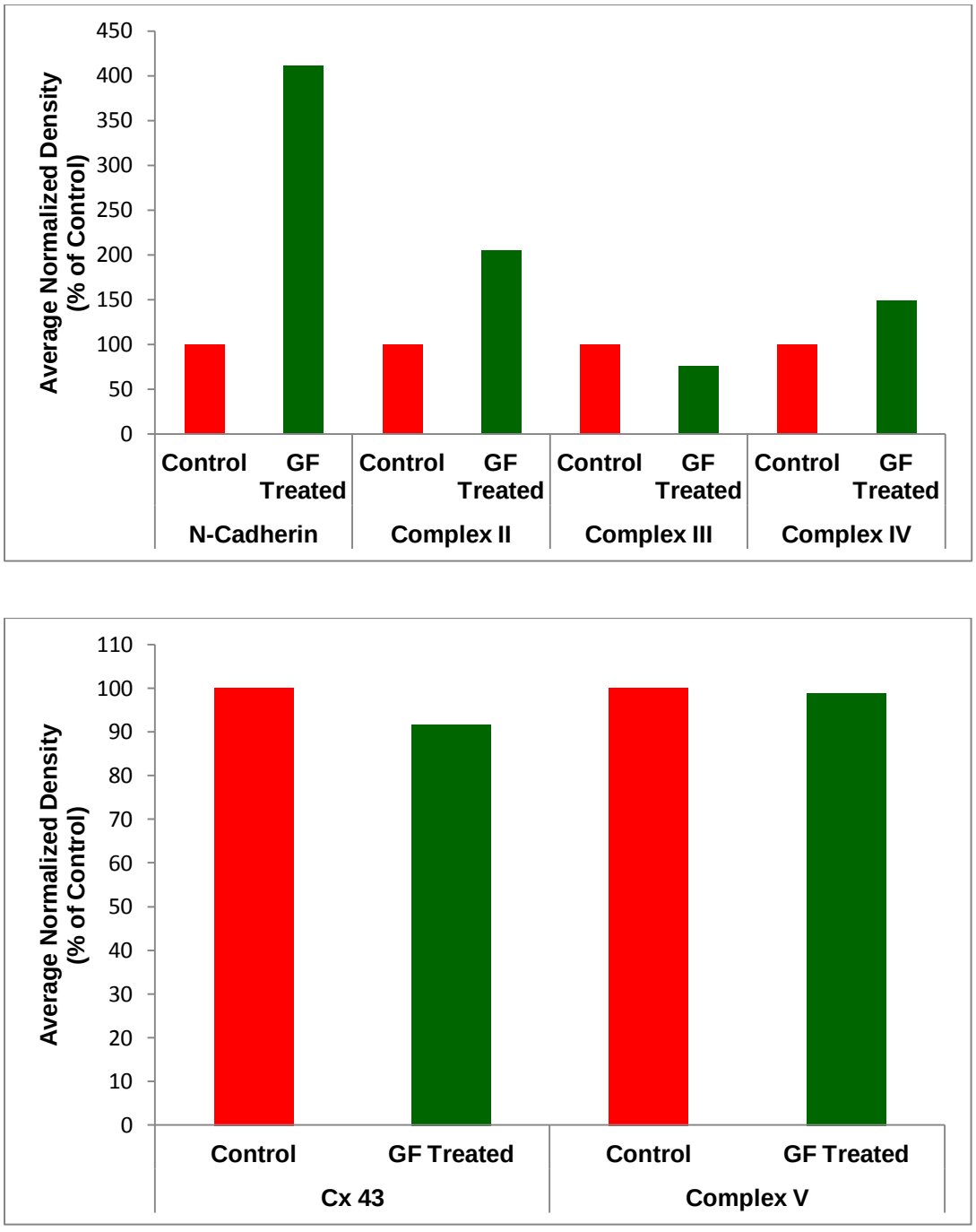

Figure 9: Cardiac and Mitochondrial Protein Expression in GF Model. Top graph: Protein expression of N-Cadherin and mitochondrial ETC complexes II-IV. Data represents the average normalized density of 4 separate experiments (n = 4) expressed as a percent of the control. **Bottom graph:** Protein expression of Cx 43 and mitochondrial ETC complex V. Data represents the average normalized density of 3 separate experiments (n = 3) expressed as a percent of the control.

C. O_2 Consumption Experimental Data

In Figure 10, a representative O_2 consumption experiment conducted in the 2.5 week GF treated model is shown. The top panel shows the O_2 concentration in the chambers of the Oroboros O_2K Oxygraph System. Over time, the top panel shows a decrease in O_2 concentration. By taking the negative value of the slope in the top panel, the value for the O_2 consumption rate is known and visible in the bottom panel. In O_2 consumption experiments, addition of substrates tends to increase O_2 consumption while inhibitors such as Rotenone and Oligomycin tend to decrease O_2 consumption. For the representative experiment shown in Figure 10, the rate of O_2 consumption is higher in GF treated hMSCs compared to control hMSCs throughout the entire experiment.

In Figure 11, the results of all viable O_2 consumption experiments used with the control and GF treated hMSCs (2.5 weeks) are represented graphically. In Figure 11, there was increased O_2 consumption across all substrate combinations for the GF treated hMSCs (2.5 weeks) compared to control hMSCs. Substrate combinations involving complex II showed the most noticeable increases in the GF treated hMSCs compared to control hMSCs during O_2 consumption experiments. The increases in O_2 respiration were due to the addition of specific mitochondrial ETC substrates and inhibitors, thus any changes in O_2 consumption were strictly mitochondrial. However, once again like qRT-PCR, the results were variable in the O_2 consumption experiments; thus, any increases seen in the GF treated hMSCs compared to control hMSCs were not significant ($p > 0.05$).

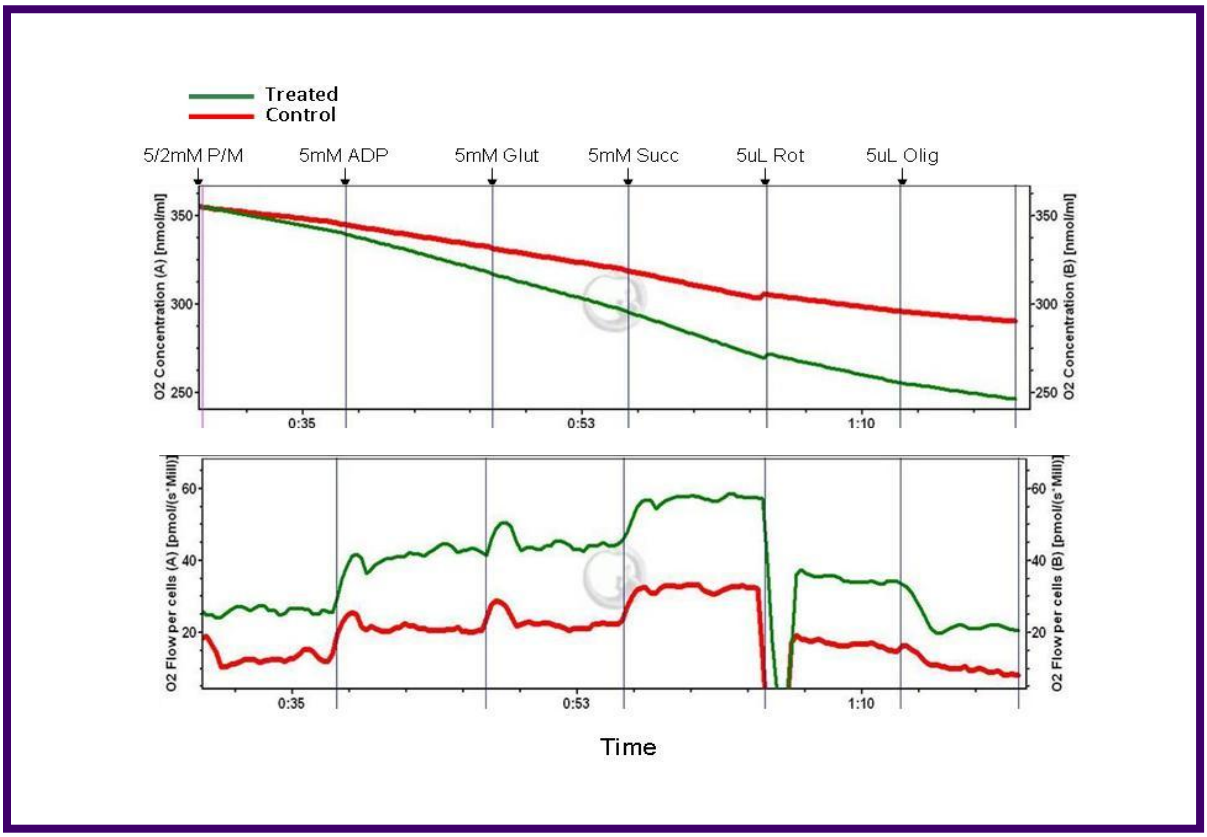

Figure 10: Representative Results of O_2 consumption experiment. Top panel: O_2 concentration in the sealed incubation chamber of the Oroboros O_2K Oxygraph System. **Bottom panel**: rate of O_2 consumption in the hMSCs. Notice the rate of O_2 consumption is higher in GF treated hMSCs throughout the entire experiment.

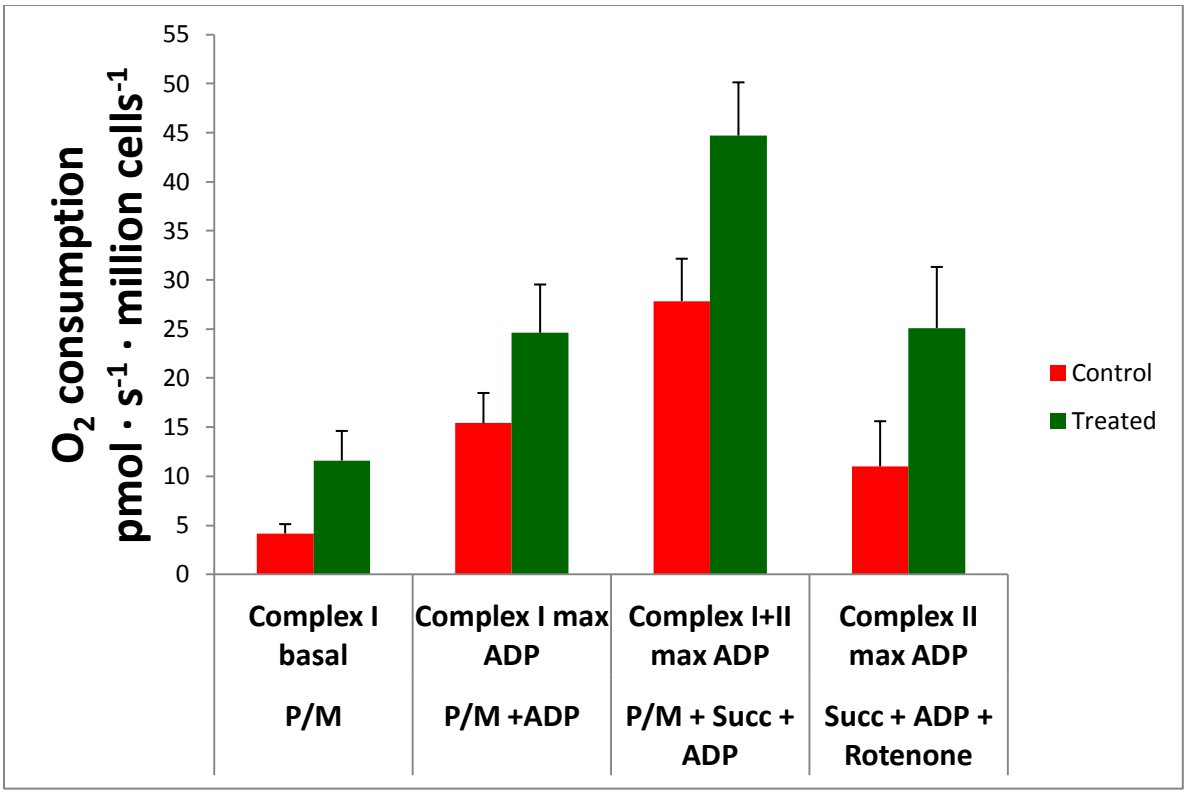

Figure 11: **GF treatment on O_2 consumption in hMSCs.** O_2 consumption rates were assessed in the presence of excess concentration of Pyruvate and Malate alone (P/M), Pyr/Mal with maximum concentration of ADP (P/M + ADP), Pyr/Mal and ADP with Succinate, (P/M + Succ + ADP), and Succinate with ADP (Succ + ADP + Rotenone). Rotenone acts as a Complex I inhibitor. Note the increase in rates of O_2 consumption with 2.5 weeks of GF treatment across all substrate combinations even though there was no significant difference in O_2 consumption between control and GF treated hMSCs. The bars show mean ± SEM. (n=3).

D. 2D and 3D Imaging with Reconstruction Analysis

The results from 2D imaging showed a change in mitochondrial localization for control and GF treated hMSCs with increased time in culture. The results from 3D imaging and reconstruction followed by analysis revealed a unique mitochondrial morphology in GF treated hMSCs compared to control hMSCs.

1. 2D Imaging – Mitochondrial Localization

The results from 2D imaging are shown in Figure 12. At early culture times (4 days in culture), both the control and GF treated hMSCs showed perinuclear mitochondrial localization. In both the control and GF treated hMSC groups at later culture times (11 days in culture), mitochondria distributed throughout cytoplasm and appeared to show increased mitochondrial content. No method was available to measure any differences between control hMSCs and GF treated hMSCs, thus leaving this analysis as a potential future study.

2. 3D Imaging and Reconstruction

The computer generated 3D reconstructions for control and GF treated hMSCS are shown in Figure 13. A crossection image is shown in Figure 13 as a 3D confocal image slice and as part of a computer generated reconstruction for control and GF treated hMSCs. In addition, a 3D computer generated surface rendering is also being shown in Figure 13.

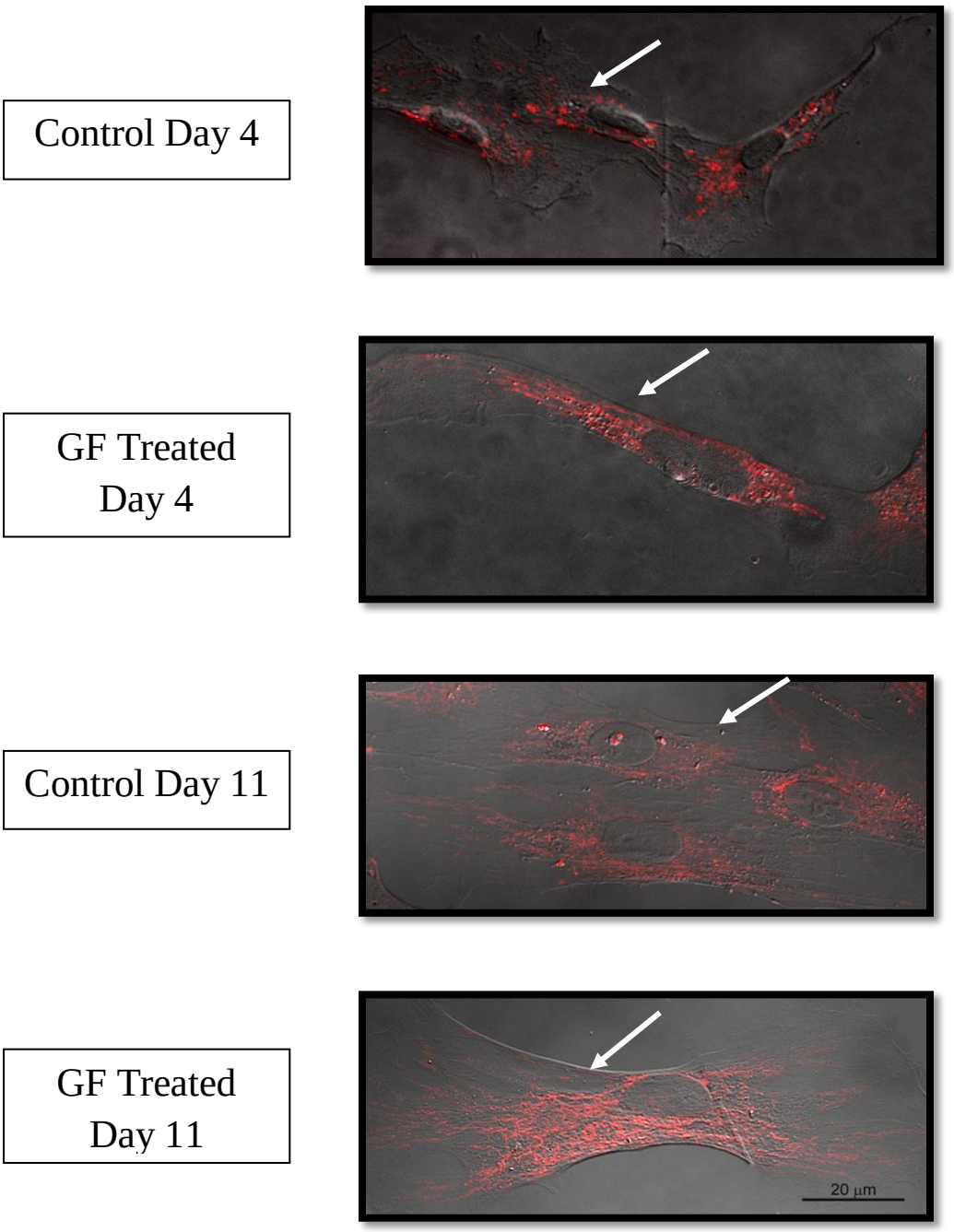

Figure 12: 2D Imaging Results showing Mitochondrial Localization in GF Treated Model. In early cultures, mitochondria were less abundant and perinuclearly localized. At 11 days in culture, mitochondrial content increased and distributed throughout the cytoplasm.

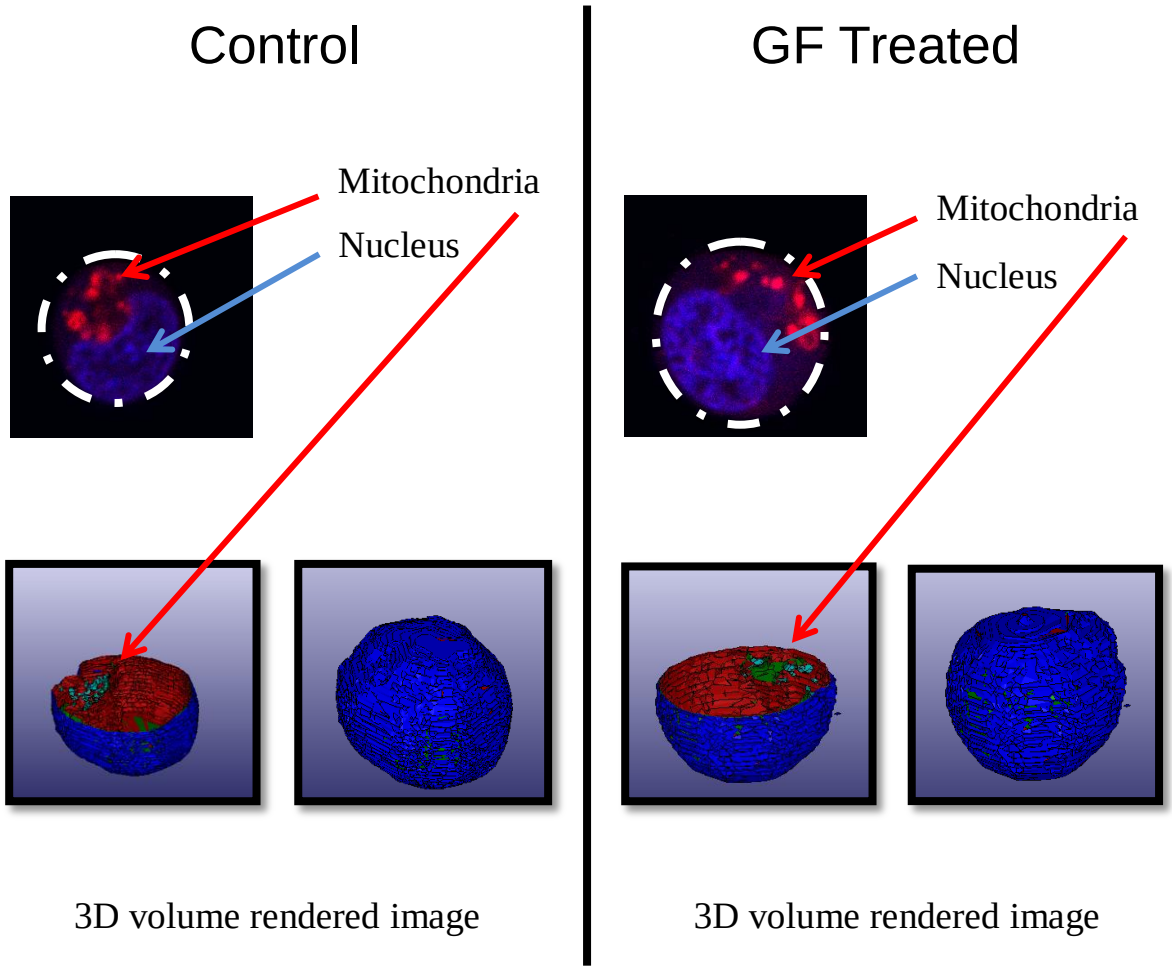

Figure 13: 3D hMSC Imaging and Reconstruction. Control: Top left image shows a 1 µm crossection of a control hMSC. The outline of the cell is shown by the white dashes. The mitochondria are shown in red, and the nucleus is shown in blue. The bottom left image shows a computer generated 3D reconstruction of the cell at the same crossectional area with the mitochondria shown in green. The reconstruction on the right is a 3D surface rendering of the cell. **GF Treated:** Similar images of GF treated hMSCs are shown in the right panel.

3. 3D Reconstruction Morphological Analysis

The 3D reconstructions were used to quantify mitochondrial morphology. Over 80 cells were imaged for each group in Model # 2 (control and GF treated hMSCs); however, Table 6 shows the preliminary analysis results of overall cell morphology for 25 hMSCs each. The cell surface area and volume were used as controls in this experiment to ensure no difference in cell size between control and GF treated hMSCs. Nuclear surface area and volume showed a statistical significant increase in GF treated hMSCs compared to control hMSCs. The nucleus to cell volume ratio showed a statistical significant increase in GF treated hMSCs compared to GF treated hMSCs. The index of surface irregularity in Table 6 refers to irregularities such as bumps, roughness, or folds on a smooth surface. A large value for the index of surface irregularity indicates many irregularities on a surface. No significant difference was measured for the index of surface irregularity in the nucleus for control and GF treated hMSCs.

Mitochondrial surface area and volume showed a statistical significant increase in GF treated hMSCs compared to control hMSCs. The surface to volume ratio of mitochondria showed an increase that was close to significance in GF treated hMSCs compared to control hMSCs ($p = 0.054$). No significant difference was measured for the mitochondrion to cell volume ratio between GF treated hMSCs and control hMSCs.

Table 6: 3D Morphological parameters

PARAMETER	UNIT	MEAN ± STARDARD DEVIATION		p
		Control (n=25)	GF treated (n=25)	
Cell surface area	μm^2	30.561±8.93	28.261±9.59	0.438
Cell volume	μm^3	454.15±161	384.25±163	0.438
Nucleus				
Nuclear surface area	μm^2	18.900±4.98	24.257±9.100	**0.026**
Nuclear volume	μm^3	194.50±91.481	281.30±126.778	**0.018**
Volume ratio of nucleus to cell	-	0.4274±0.2122	0.7225±0.158	**<0.001**
Index of surface irregularity of nucleus	$\mu m^{-1/2}$	201.41±36.3	204.52±54.4	0.883
Mitochondria				
Mitochondrial surface area	μm^2	90.593±151	277.15±317	**0.023**
Mitochondrial volume	μm^3	71.20±109.314	205.30±228.853	**0.023**
Index of surface irregularity of mitochondria	$\mu m^{-1/2}$	1038.7±1135	2068.5±1783	**0.036**
Surface to volume ratio of mitochondria	μm^{-1}	0.9456±0.261	1.1167±0.282	**0.054**
Volume ratio of mitochondrion to cell	-	0.2048±0.374	1.0359±2.031	0.080

IV. DISCUSSION

A. Conclusions

Overall, the main objective of this study was to improve the basic understanding of adult stem cell differentiation in cardiac tissue regeneration and repair by investigating the role of mitochondrial biogenesis in adult hMSC differentiation and acquisition of a cardiac phenotype in a simulated cardiac co-culture microenvironment (Model # 1) and in a GF treated monoculture model (Model # 2). To that end, the main results of this investigation for Model # 1 and Model # 2 are summarized below:

- Model # 1 (Co-cultured hMSCs)
    - Increased cardiac and mitochondrial gene expression
- Model # 2 (GF treated hMSCs)
    - Increased mitochondrial gene expression
    - Increased cardiac and mitochondrial protein expression
    - Increased mitochondrial O_2 consumption
    - Increased mitochondrial surface area, volume, and surface irregularity

In Model # 1 and Model # 2, mitochondrial biogenesis is evident. For Model # 1, mitochondrial gene expression of TFB1M and UQCRC1 was significantly increased in co-cultured hMSCs vs. control hMSCs. In Model # 2, no difference in mitochondrial gene expression was observed at 48 hours suggesting that mitochondrial biogenesis signaling may occur at different time points in Model # 1 and Model # 2. For Model # 2 at 2.5 weeks, mitochondrial gene expression showed a significant increase in TFB1M. Western blot analysis suggests a trend in protein expression for complexes II and IV.

Increased mitochondrial O_2 consumption for all mitochondrial substrate combinations was observed in 2.5 week GF treated hMSCs compared to control hMSCs where substrate combinations utilizing complex II were closest to significance. 3D imaging, reconstruction, and analysis revealed a unique mitochondrial morphology in GF treated hMSCs. Mitochondrial surface area and volume along with increased mitochondrial surface irregularities showed significant increases in GF treated hMSCs compared to control hMSCs. In summary, Model # 1 showed early signaling and changes of mitochondrial biogenesis at 48 hours. While mitochondrial biogenesis was not observed at this early time point in Model # 2, it was evident at 2.5 weeks in GF treated hMSCs.

Model # 1 and Model # 2 show changes in mitochondrial biogenesis. However, was this biogenesis involved in hMSC acquisition and differentiation into a cardiac phenotype? In Model # 1, cardiac gene expression of MEF2C was significantly increased in co-cultured hMSCs vs. control hMSCs. But, in Model # 2, cardiac gene expression did not change over 2.5 weeks. Furthermore, cardiac protein expression of N-cadherin only suggested a trend for increased expression in GF treated hMSCs. In addition, in Model # 1, mitochondrial ETC complex III expression may play a role in early hMSC differentiation into a cardiac phenotype. In Model # 1, UQCRC1 (complex III subunit) gene expression was significantly increased in co-cultured hMSCs vs. control hMSCs. In Model # 2, no difference in UQCRC1 gene expression was found at 48 hours and 2.5 weeks. Furthermore, no difference in complex III protein expression was observed for Model # 2 at 2.5 weeks suggesting no differences overall for complex III expression in Model # 2 and a potential reason for the lack of cardiac-like differentiation in GF treated hMSCs. Complex III upregulation may be necessary for hMSC differentiation in Model #

1 because complex III expression has been shown to be necessary for embryonic stem cell and hMSC differentiation into lineages such as fat, bone, and muscle ((Spitkovsky et al. ; Tormos et al. 537-544; Varum et al. 142-156). Future studies are needed to explore the importance of complex III in hMSC differentiation in Model # 1. Based on the results of this investigation, Model # 1 may be a better model for directing hMSCs to a cardiac like fate compared to Model # 2. Thus, Model # 1 supported the hypothesis that mitochondrial activity and biogenesis would be enhanced when hMSCs were directed towards a cardiac-like fate while Model # 2 did not fully support this hypothesis.

Model # 2 suggests enhanced mitochondrial biogenesis with increased time in culture when treated with GFs may lead to improved hMSC survival and proliferation. One study has shown that pre-treatment with GFs improves therapies when hMSCs are transplanted into the cardiac environment by enhancing engraftment and by limiting infarct size and apoptosis; this study has proposed increased gap junction function to be a factor of these therapeutic enhancements without providing strong support for its causal connection in improved therapies (Hahn et al. 933-943). However, mitochondrial biogenesis in GF treated hMSCs may also be a factor in improved hMSC therapies based on Model # 2's results. The role of mitochondrial biogenesis in adult stem cell survival and therapies for cardiac tissue regeneration and repair has not been explored. Thus further studies must determine if a relationship exists between enhanced gap junction function and enhanced mitochondrial biogenesis in stem cell survival when transplanted into a cardiac environment.

B. Study Limitations

There were study limitations present in this investigation. Many of these limitations were from Model # 1 (the 48 hour Co-culture model). The short culture time of Model # 1 may be considered one of its limitations. The culture time of the co-culture model was short (only 48 hours) compared to Model # 2 (the 2.5 weeks GF model) due to several reasons. The first reason for this short culture time in Model # 1 was attributable to the strong connections between the hMSCs and the cardiomyocytes developed over time in this model. The cells become intertwined and difficult to separate for other experiments when allowed to grow in co-culture for long periods of time. On the other hand, at earlier time points in the co-culture model, the hMSCs were more mobile thus easing the separation process from cardiomyocytes.

The second reason for keeping a short culture time in this model was due to a dilution effect created by the hMSCs. From previous investigations, it was hypothesized that direct cell-cell contact with cardiomyocytes (and not juxtacrine and paracrine factors) in the co-culture model is necessary for hMSC acquisition and differentiation of a cardiac-like phenotype (Muller-Borer et al. e38454). With time in culture, hMSCs grow and proliferate. Due to hMSC proliferation, a fixed amount of hMSC-cardiomyocyte cell contacts in co-culture are outnumbered by proliferating hMSCs not in contact with the cardiomyocytes. As hMSCs continued to increase, the hMSCs (showing potential to differentiate into cardiomyocytes) in contact with the cardiomyocytes were diluted by the influx of other hMSCs. This dilution affected other experiments such as gene expression causing misrepresentation of hMSCs desired for study. Furthermore, if this culture was prolonged, hMSCs began to take most of the nutrients and space present for both cell

types in co-culture. The cardiomyocytes began to die from lack of nutrients by the aggressive growth and proliferation of hMSCs.

The short culture time created another limitation in the co-culture model. A low hMSC yield due to the short culture time was the second limitation of this model. By having a short culture time, proliferation of hMSCs was limited and fewer hMSCs were available for analysis. The low yield of hMSCs was also caused by several other reasons. The 1:10 ratio of hMSCs to cardiomyocytes was one of the reasons why the co-culture model yielded a low number of hMSCs. The addition of a small number of hMSCs to a large number of cardiomyocytes for a short culture time did not produce enough hMSCs for many experiments. Another reason for low cell yield in this model was due to the separation of hMSCs from cardiomyocytes. The hMSC separation from cardiomyocytes greatly reduced the amount of hMSCs grown in co-culture. Different separation methods were evaluated to gain the highest hMSC yield.

Two different attempts were made at separating the hMSCs from the cardiomyocytes. The first attempt included FACS sorting hMSCs. Two cell groups were used to evaluate FACS sorting as a viable separation method of the hMSCs from the cardiomyocytes. Both cell groups were hMSC monocultures grown at incubator conditions with full media for 2.5 weeks like the control hMSCs from Model # 2. The first group of cells labeled as FACS Sorted hMSC Monoculture was FACS sorted. The second group of cells labeled as Non-sorted hMSC Monoculture was not FACS sorted. After FACS sorting, the FACS Sorted hMSC Monoculture returned a low cell yield limiting other follow-up experiments. Because of a low cell yield, the viability of the sorted hMSCs and the experimental technique of the FACS separation were questioned.

Thus, evaluation of FACS sorting hMSCs on hMSC's metabolic activity and viability was completed by a mitochondrial O_2 consumption experiment between the Non-sorted hMSC Monoculture and the FACS Sorted hMSC Monoculture. The Results of the O_2 consumption experiment are shown in Figure 14.

From the Results shown in Figure 14, FACS Sorted hMSCs were more metabolically active compared to hMSCs that were not FACS sorted. Higher rates of O_2 consumption were seen in the FACS sorted hMSCs during the addition of the substrate ADP and the complex II substrate Succinate. From the Results in Figure 14, it was evident that the FACS sorting selected for more robust and metabolically active hMSCs than the overall population of non-sorted hMSCs. One explanation suggested for this odd occurrence is due to the heterogeneity of the hMSC population before FACS sorting. The non-sorted hMSCs may have the ability to differentiate into many divergent cell types with different metabolic profiles. FACS sorting possibly selected for a certain group of hMSCs thus creating a small homogeneous population of hMSCs with a higher metabolic profile compared to the large heterogeneous population of non-sorted hMSCs.

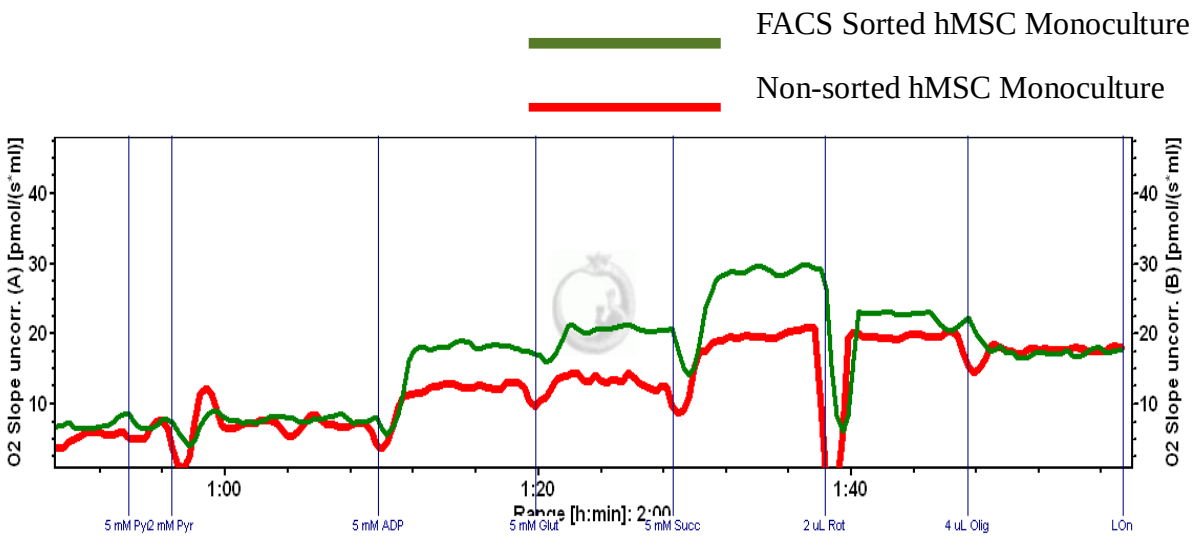

Figure 14: O_2 Consumption of FACS Sorted vs. Non-sorted hMSC Monocultures. Note the higher respiration of FACS sorted hMSCs with the addition of ADP and the complex II substrate Succinate.

FACS was also used to sort hMSCs in Model # 1. When control (monoculture) and co-cultured hMSCs were separated by FACS, both groups of hMSCs also showed low cell yield similar to the sorted hMSC monoculture (2.5 week culture). The co-cultured hMSCs with cardiomyocytes approached only a 30% cell yield after separation by FACS. Due to a low cell yield in both the monoculture hMSCs and the co-cultured hMSCs, and higher metabolic profiles established in the hMSC monocultures from FACS sorting; FACS separation technique was not an ideal method due to limited number and skewed representation of hMSCs that arose from it.

The second attempt at separating the hMSCs from the cardiomyocytes in co-culture was the CD 90 magnetic bead separation. The cell yield using the magnetic bead separation approached 50% in Model # 1. Therefore, hMSC separation from cardiomyocytes with CD 90 magnetic beads returned a higher yield of cells compared to FACS separation. Because of the higher yield of hMSCs compared to FACS separation, magnetic bead separation was used to separate hMSCs from cardiomyocytes for this investigation. However, magnetic bead separation also produced an inadequate hMSC yield from co-culture separation for other experiments.

C. Future Studies

1. Model # 1 – 48 Hour Co-culture Model

Due to study limitations in the co-culture model, expansion of experimental measurements or substitution of this model must be done. For future studies, experimental measurements can be expanded in Model # 1 even with study limitations of low cell yields. In order to expand experimental measurements with low hMSC yield, microscopy is one possibility for this model. Microscopy uses fewer cells than other experiments such as qRT-PCR, western blots, and mitochondrial O_2 consumption; thus, making it an optimal choice of study for Model # 1. Two microscopy investigations are suitable for expanding experimental measurements in this model.

The first microscopy investigation should include 3D imaging and reconstruction. By taking 3D images on a confocal microscope, valuable data concerning mitochondrial morphology may be quantified as done in Model # 2 using the computer generated reconstructions. In addition, 2D imaging may also be completed in Model # 1 to provide knowledge on mitochondrial localization. Differences at early culture times in control and co-cultured hMSC mitochondrial distribution will be elucidated. Furthermore, 2D imaging can also be completed at later culture times because co-cultured hMSCs do not need to be separated from cardiac myocytes as done for qRT-PCR. The hMSCs are transduced with a lentiviral vector encoding for the fluorescent protein, dsRed, which targets mitochondria and identifies hMSCs from cardiac myocytes in confocal microscopy. By completing the

first microscopy investigation, further data will be established on the similarities of mitochondrial distribution and morphology in Model # 1 and Model # 2.

The first microscopy investigation can be completed to provide data on mitochondrial distribution and morphology, while the second microscopy investigation should be completed to provide data on mitochondrial master regulator proteins necessary for mitochondrial biogenesis. By studying the behavior of these master regulators in microscopy, further evidence could be used to potentially support the results of qRT-PCR in Model # 1. One potential example for the second microscopy investigation is to study the location of NRF-1 in co-cultured hMSCs vs. control hMSCs. The results of qRT-PCR revealed no significant differences in NRF-1; however, lack of difference in expression does not explain the location of NRF-1 in hMSCs. In the presence of intracellular Ca^{2+} or potentially with Ca^{2+} oscillations, NRF-1 moves from the cytoplasm into the nucleus to turn on genes further down in the mitochondrial biogenesis signaling pathway (Chau, Evans, and Scarpulla 6999-7006; Gugneja, Virbasius, and Scarpulla 5708-5716; Gugneja and Scarpulla 18732-18739; Murakami et al. 113-122; Virbasius, Virbasius, and Scarpulla 2431-2445). By having a higher nuclear to cytosolic ratio of NRF-1 in co-cultured hMSCs vs. control hMSCs (with a co-culture model known for Ca^{2+} oscillations) suggests NRF-1 is involved with mitochondrial biogenesis even though no difference in gene expression was revealed with qRT-PCR (Muller-Borer et al. e38454). If what is proposed for NRF-1 has been found to be supported in Model # 1, then it immediately suggests a mitochondrial biogenesis signaling pathway that may be involved in the cardiac differentiation of hMSCs.

Substitutions in the co-culture model must be done in order to further study and elucidate the mitochondrial biogenesis pathway in hMSC acquisition and differentiation of a cardiac phenotype. One substitution in Model # 1 that can be completed may be siRNA experiments. CAMTA-1, a cardiac gene evaluated in Model # 1, has been shown to be necessary in hMSC differentiation into a cardiac like phenotype in Model # 1 by loss of function siRNA experiments (Muller-Borer et al. e38454). When CAMTA-1 gene expression was knocked down by CAMTA-1 siRNA, cardiac gene expression was also minimized. The CAMTA-1 siRNA provides an opportunity for future studies in determining if the mitochondrial biogenesis signaling pathway is directly integrated in hMSC cardiac-like differentiation of Model # 1. After CAMTA-1 siRNA is used for hMSCs in co-culture and the second microscopy investigation is completed in Model # 1, qRT-PCR can be used to evaluate NRF-1 gene expression, and microscopy can be used to evaluate NRF-1's nuclear to cytosolic ratio in order to determine if CAMTA-1 is necessary for NRF-1 gene expression and recruitment to the nucleus for activation of the mitochondrial biogenesis signaling pathway. In addition, other mitochondrial gene expression (specifically UQCRC1) may be evaluated in order to determine if CAMTA-1 gene expression is necessary to turn on other mitochondrial genes such as UQCRC1. After determining UQCRC1's involvement in hMSC acquisition and differentiation into a cardiac-like phenotype, the necessity of UQCRC1 in this process can be verified by using UQCRC1 siRNA (or other complex III genes) in Model # 1 and evaluating differences in cardiac gene expression.

If the future studies proposed are completed, the importance of mitochondrial biogenesis in this model will be clarified. Thus, from the results obtained in this investigation and the results found in the literature, the signaling pathway in Figure 15 is hypothesized. This hypothesis suggests intracellular Ca^{2+} and Ca^{2+} oscillations turn on CAMTA-1, and CAMTA-1 activates cardiac gene expression in Model # 1. Future studies will either support the hypothetical signaling pathway or reject it by determining if CAMTA-1 is necessary for mitochondrial gene expression (and NRF-1 localization) and if mitochondrial gene expression is necessary for cardiac gene expression and differentiation.

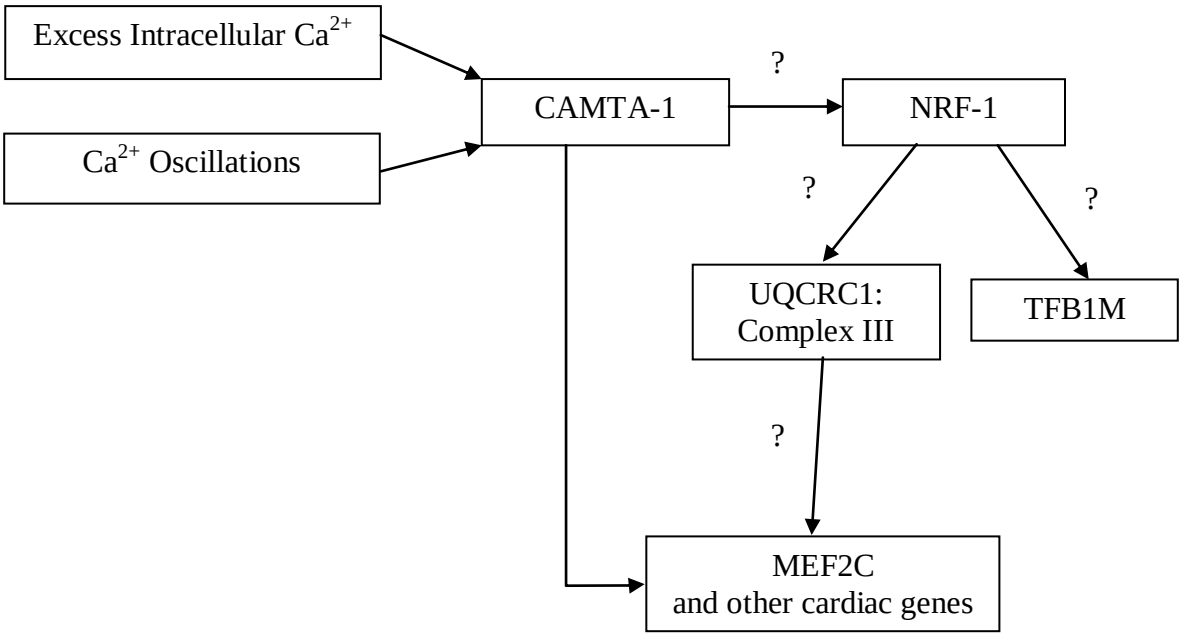

Figure 15: Hypothetical Mitochondrial Biogenesis Signaling Pathway in Model # 1. Ca^{2+} has been known to activate CAMTA-1 and eventually MEF2C and other cardiac genes. However, mitochondrial biogenesis in this differentiation pathway is not known for this model. Results from this investigation and future studies propose CAMTA-1 maintains NRF-1 gene expression and localization. NRF-1 localization in the nucleus suggests activation of mitochondrial biogenesis pathway by turning on the genes TFB1M and UQCRC1. Furthermore, UQCRC1 and other complex III genes are necessary for activating MEF2C and other cardiac genes.

2. Model # 2 – GF Treated Model

Future studies can also be completed in Model # 2. The literature has shown that hMSCs treated with GFs express enhanced gap junction function, and this enhanced gap junction function increases therapeutic efficiency by reducing infarct size and improving cardiac function in a rat myocardial infarction model (Hahn et al. 933-943). However, this enhanced gap junction function was only observed after the GF treated hMSCs were co-cultured with rat cardiac myocytes or when placed in the myocardial infarction model (Hahn et al. 933-943). No enhanced gap junction function and no difference in Cx 43 protein expression were observed when GF treated hMSCs were not co-cultured with cardiac myocytes (Hahn et al. 933-943). No difference in Cx 43 protein expression in the literature correlates with results of Cx 43 gene and protein expression in this investigation for Model # 2.

Future studies can determine if gap junction function is enhanced solely with GF treatment (and not supplemented by co-culture with cardiac myocytes) to ease pre-treatment for future therapies. Even with no differences in Cx 43 gene and protein expression, other measurements can be completed to determine if gap junction function is enhanced solely with GF treatment. These measurements include Fluorescence Recovery After Photobleaching (FRAP) and immuoncytochemistry.

Fluorescence Recovery After Photobleaching (FRAP) should be completed to determine overall physiological gap junction function. If there is increased fluorescence recovery in one group of cells compared to a second group of cells after photobleaching with a confocal microscope, then the first group would show

enhanced gap junction function compared to the second group potentially due to open and active gap junctions. Preliminary results were obtained for FRAP in this investigation for Model # 2. When FRAP was conducted with an on-stage incubator system, a difference in the rate of recovery and amount of fluorescent intensity was measured. At incubator conditions (37°C and 5% CO_2), the GF treated hMSCs showed a higher rate of fluorescent recovery as shown in Figure 16.

Another way to represent the FRAP experiment is by observing FRAP kinetics. FRAP kinetics should be simplified to the following equation if gap junction conductance is considered the rate-limiting step:

$$\text{Equation 1: } \frac{C_e - C_t}{C_e - C_0} = e^{-kt}$$

In Equation 1, C_e, C_0, and C_t are the dye concentrations in the cell at equilibrium, initial time, and time, respectively (Wade, Trosko, and Schindler 525-528; Abbaci et al. 50-61). Because this is a FRAP experiment, the measured variable at various times is the fluorescent intensity. Due to the relationship between the dye concentration in the cell and the fluorescent intensity in the cell, fluorescent intensity (the measured variable) can replace the dye concentration variable in Equation 1, thus creating Equation 2 below.

$$\text{Equation 2: } \frac{F_b - F_t}{F_b - F_0} = e^{-kt}$$

In Equation 2, F_b is the fluorescent intensity before photobleaching, F_0 is the fluorescent intensity immediately after photobleaching, and F_t is the fluorescent

intensity at any given time after photobleaching (Wade, Trosko, and Schindler 525-528; Abbaci et al. 50-61).

When the rate constant for a specific transfer of fluorescent molecules is large, the rate of transfer is fast. Results of the rate constants K1 and K2 are shown in Figure 17. Notice the values for the rate constants K1 and K2 are significantly increased with GF treatment as shown in Figure 17. These results suggest the exchange rate of fluorescent molecules is larger with GF treatment. Increased fluorescent recovery in GF treated hMSCs is due to facilitated diffusion caused by open gap junctions and could be due to increased gap junctions compared to the control hMSCs.

Several experimental controls should be observed to validate any results from FRAP experiments. The experimental control observed above in Figure 18 is the depth of photobleaching. The depth of photobleaching is the change of normalized fluorescent intensity from the original percent value to the first measured normalized intensity percent value immediately at the end of photobleaching. If the depth of photobleaching is significantly different between groups, then the rate of recovery and the intensity of fluorescence recovered may be affected resulting in skewed data. Figure 18 shows no significant difference in the depth of photobleaching between the control and GF treated groups of hMSCs. The second experimental control observed is the bleach time. If the bleach times are significantly different, then the increased rate of recovery and an increased fluorescent intensity recovered can be due to a shorter bleach time. Figure 19 shows no significant difference in the bleach time between the control and GF treated groups.

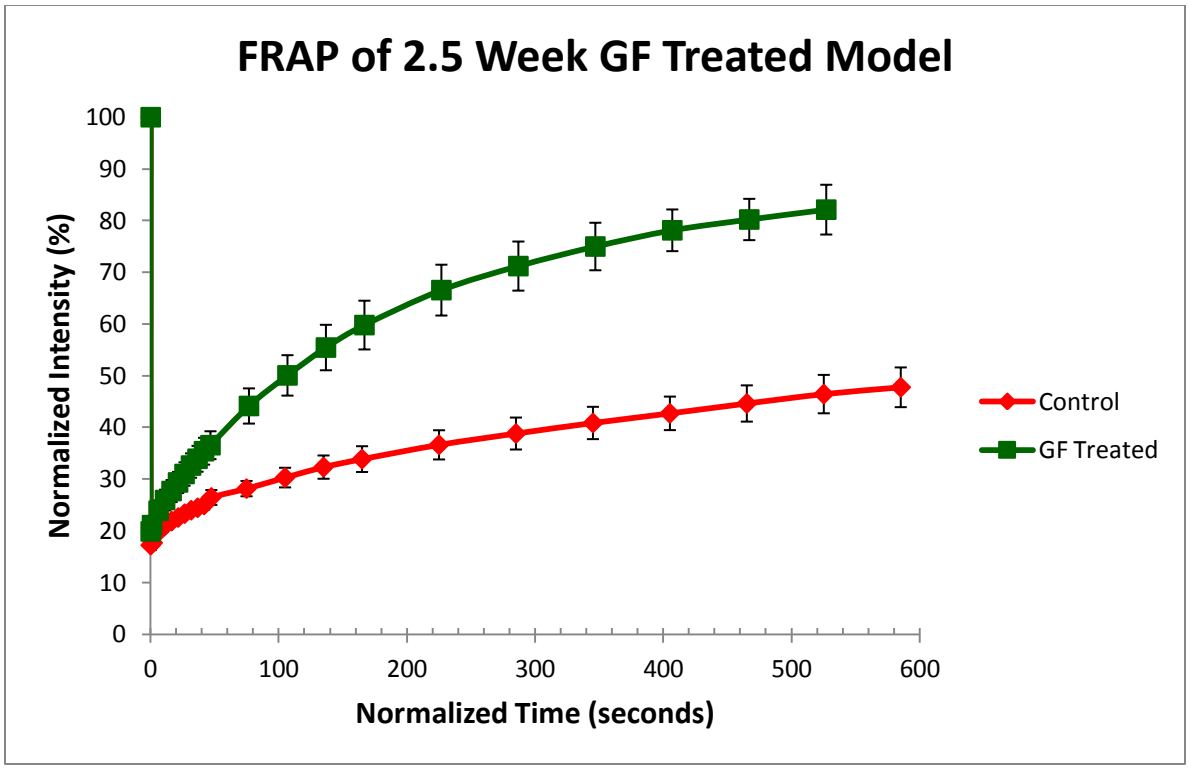

Figure 16: Preliminary FRAP Results on 2.5 Week GF Treated Model (Model # 2). Cells were labeled with the cytosolic dye Calcein AM. The FRAP procedure was completed with a staging incubator system on a laser scanning confocal microscope (LSM 710) where the conditions were at 37°C and 5% CO_2. Note the increase and the speed in FRAP with GF treatment. Results are represented as n = 1 (5 observations per group).

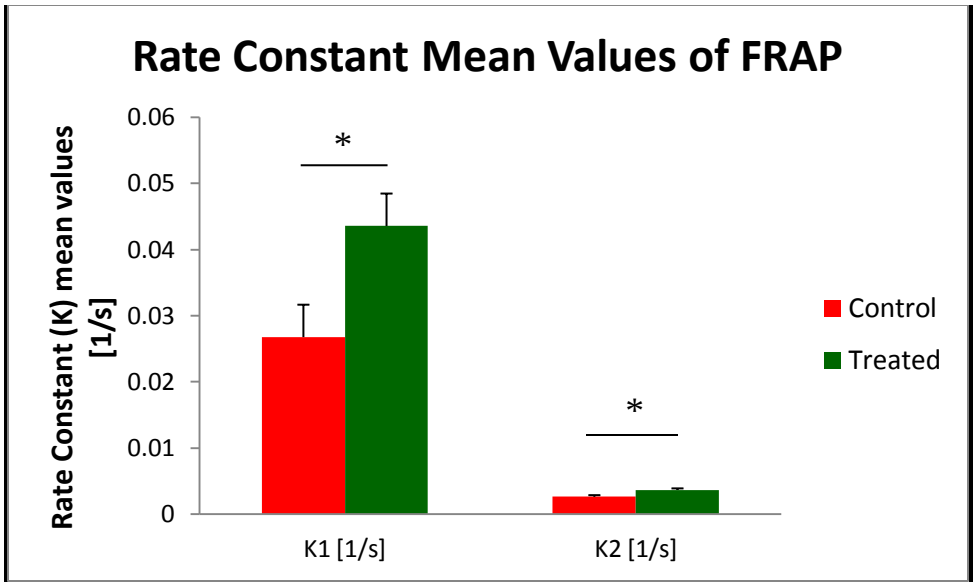

Figure 17: Rate Constant Mean Values of FRAP. The mean of the rate constants K1 and K2 are graphed above with the units [1/s]. The high value rate constant indicates a fast fluorescence recovery. Note the GF treated group shows larger values for the rate constants. The bars show mean ± SEM. A significant difference between the control group and the GF treated group for both rate constants K1 and K2 was observed ($p < 0.05$). Results are represented as n = 1 (5 observations per group).

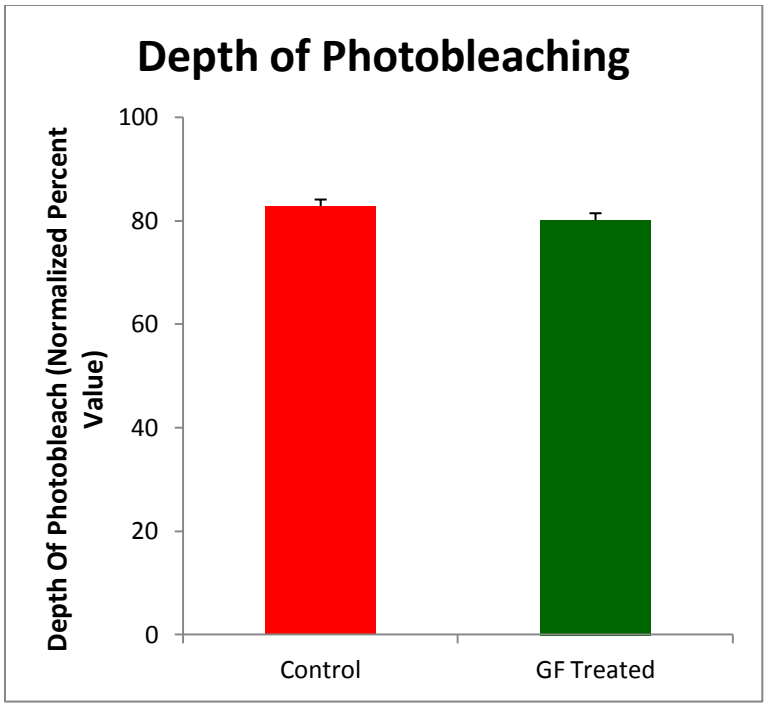

Figure 18: Depth of Photobleaching in FRAP. The depth of photobleaching is the initial loss of fluorescence caused by photobleaching. A Significant difference in depth of photobleaching may skew FRAP results. Thus having a similar depth of photobleaching serves as an experimental control. There was no significant difference in the control group versus the GF treated group ($p > 0.05$). The bars show mean ± SEM. Results are represented as n = 1 (5 observations per group).

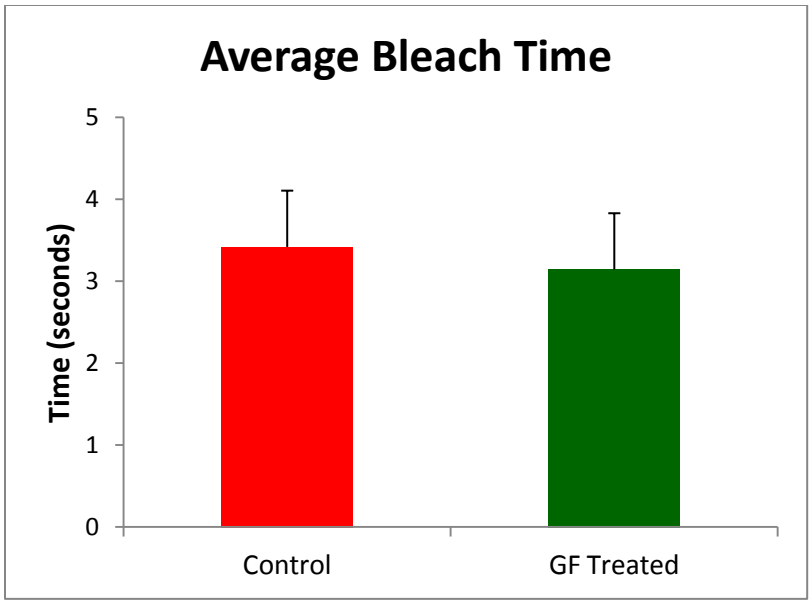

Figure 19: Average Bleach Time in FRAP. The average bleach time is the time for photobleaching to occur. Similar to the depth of photobleaching, significantly different average bleach times may skew FRAP results. Thus having a similar average bleach time serves as an experimental control. There was no significant difference in control hMSCs versus GF treated hMSCs ($p > 0.05$). The bars show mean ± SEM. Results are represented as n = 1 (5 observations per group).

The speed and increase in FRAP along with increased rate constants with GF treatment suggest enhanced gap junction function in GF treated hMSCs vs. control hMSCs. FRAP will have to be repeated in order to establish reproducibility on enhanced gap junction function. If enhanced gap junction function is evident after repeating the FRAP experiment, then specific gap junctions being enhanced from solely GF treatment must be determined. The literature has suggested Cx 43 to be one of these enhanced gap junctions when GF treated hMSCs were co-cultured with cardiac myocytes (Hahn et al. 933-943). Thus, Cx 43 may be one of the enhanced gap junctions present in GF treated hMSCs before co-culturing with cardiac myocytes. However, with no difference in Cx 43 gene and protein expression with GF treatment alone, Cx 43 is unlikely to be one of the enhanced gap junctions represented from the results of FRAP. Immunocytochemistry can be completed to confirm Cx 43 gene and protein expression.

Figure 20 shows images of control hMSCs and GF treated hMSCs stained with Cx 43. Cx 43 is represented as gap junctions with a green punctuate pattern lining the edges and connections of the hMSCs. The control hMSCs and GF treated hMSCs appear to be similar; however, no differences must be confirmed with fluorescent intensity after further image analysis. If there is no difference in control and GF treated hMSCs when FRAP has suggested enhanced gap junction function, then other cardiac gap junctions (Connexin 40 and 42) or non-cardiac gap junctions will have to be evaluated to determine the specific gap junction enhanced. If non-cardiac gap junction functions are enhanced, then data from Model # 2 suggests GF treated hMSCs are not differentiating towards a cardiac-like phenotype.

In addition to gap junction functional studies, the effects of mitochondrial biogenesis in hMSC survival and proliferation studies must be evaluated in GF treated hMSCs. One future study would be to administer mitochondrial ETC complex toxins for complex II (carboxin), complex III (antimycin A), and complex IV (cyanide and azide); and determine if GFs evaluated in this investigation recovers mitochondrial biogenesis, hMSC survival (propidium iodide, cell cycle analysis, and mitochondrial membrane potential flow cytometry assessment), and proliferation (wound healing assays). Overall, in Model # 1 and Model # 2, many future studies are pursuable based on the results implicated in this investigation.

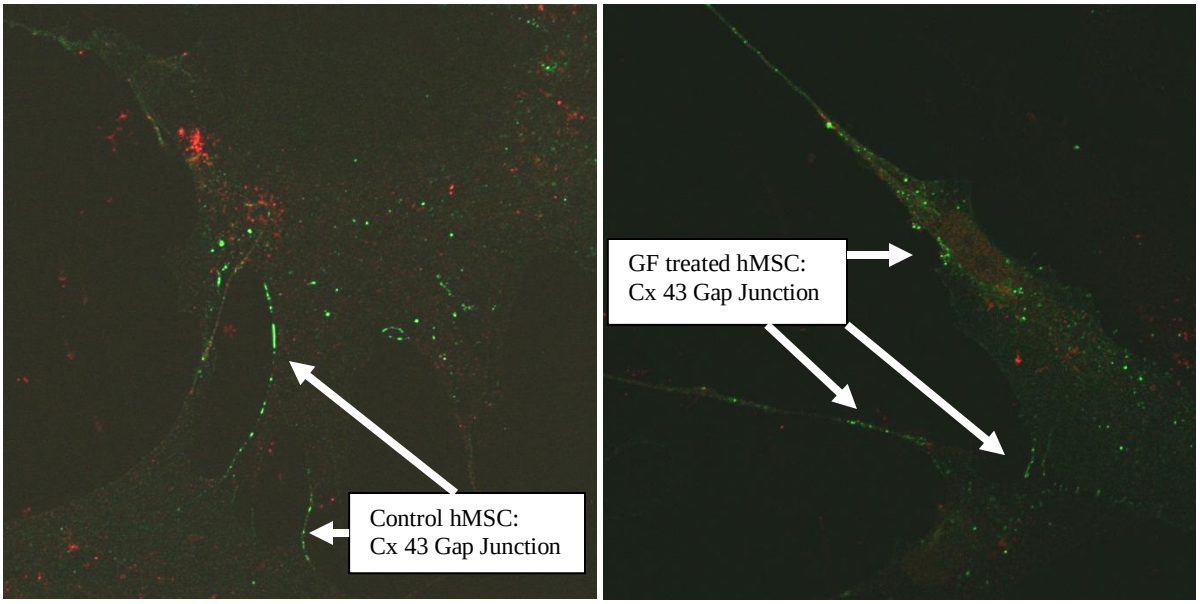

Figure 20: Immunocytochemistry of Cx 43 in Control and GF Treated hMSCs. The images were taken at 2.5 weeks. Notice the punctate green lines and connections showing the Cx 43 gap junctions along the hMSCs. The Cx 43 gap junctions in these images are shown at the edges of the hMSCs where they make connections with other hMSCs. The left image shows a control hMSC, and the right image shows a GF treated hMSC. The location of the Cx 43 gap junctions in GF treated hMSCs appears to be similar to control hMSCs.

V. **REFERENCES**

Abbaci, Muriel, et al. "Gap Junctional Intercellular Communication Capacity by Gap-FRAP Technique: A Comparative Study." *Biotechnology Journal* 2.1 (2007): 50-61. Web.

Breitbach, Martin, et al. "Potential Risks of Bone Marrow Cell Transplantation into Infarcted Hearts." *Blood* 110.4 (2007): 1362-9. Web.

Chau, C. M., M. J. Evans, and R. C. Scarpulla. "Nuclear Respiratory Factor 1 Activation Sites in Genes Encoding the Gamma-Subunit of ATP Synthase, Eukaryotic Initiation Factor 2 Alpha, and Tyrosine Aminotransferase. Specific Interaction of Purified NRF-1 with Multiple Target Genes." *Journal of Biological Chemistry* 267.10 (1992): 6999-7006. Web.

Chen, Chien-Tsun, et al. "Coordinated Changes of Mitochondrial Biogenesis and Antioxidant Enzymes during Osteogenic Differentiation of Human Mesenchymal Stem Cells." *Stem cells* 26.4 (2008): 960-8. Web.

Cho, Young Min, et al. "Dynamic Changes in Mitochondrial Biogenesis and Antioxidant Enzymes during the Spontaneous Differentiation of Human Embryonic Stem Cells." *Biochemical and biophysical research communications* 348.4 (2006): 1472-8. Web.

Chung, S., et al. "Mitochondrial Oxidative Metabolism is Required for the Cardiac Differentiation of Stem Cells." *Nature clinical practice.Cardiovascular medicine* 4 Suppl 1 (2007): S60-7. Web.

Duchen, Michael R. "Mitochondria in Health and Disease: Perspectives on a New Mitochondrial Biology." *Molecular aspects of medicine* 25.4 (2004): 365-451. Web.

Ekpenyong, Andrew E., et al. "Study of 3D Cell Morphology and Effect on Light Scattering Distribution." (2009): 73671J-. Web.

Facucho-Oliveira, J. M., et al. "Mitochondrial DNA Replication during Differentiation of Murine Embryonic Stem Cells." *Journal of cell science* 120.Pt 22 (2007): 4025-34. Web.

Fukuhara, S., et al. "Direct Cell-Cell Interaction of Cardiomyocytes is Key for Bone Marrow Stromal Cells to Go into Cardiac Lineage in Vitro." *The Journal of thoracic and cardiovascular surgery* 125.6 (2003): 1470-80. Web.

Gugneja, S., C. M. Virbasius, and R. C. Scarpulla. "Nuclear Respiratory Factors 1 and 2 Utilize Similar Glutamine-Containing Clusters of Hydrophobic Residues to Activate Transcription." *Molecular and cellular biology* 16.10 (1996): 5708-16. Web.

Gugneja, Sajiv, and Richard C. Scarpulla. "Serine Phosphorylation within a Concise Amino-Terminal Domain in Nuclear Respiratory Factor 1 Enhances DNA Binding." *Journal of Biological Chemistry* 272.30 (1997): 18732-9. Web.

Hahn, J. Y., et al. "Pre-Treatment of Mesenchymal Stem Cells with a Combination of Growth Factors Enhances Gap Junction Formation, Cytoprotective Effect on Cardiomyocytes, and Therapeutic Efficacy for Myocardial Infarction." *Journal of the American College of Cardiology* 51.9 (2008): 933-43. Web.

Kubo, Hajime, et al. "C-Kit+ Bone Marrow Stem Cells Differentiate into Functional Cardiac Myocytes." *Clinical and Translational Science* 2.1 (2009): 26-32. Web.

Labovsky, V., et al. "Cardiomyogenic Differentiation of Human Bone Marrow Mesenchymal Cells: Role of Cardiac Extract from Neonatal Rat Cardiomyocytes." *Differentiation; research in biological diversity* 79.2 (2010): 93-101. Web.

Li, X., et al. "Bone Marrow Mesenchymal Stem Cells Differentiate into Functional Cardiac Phenotypes by Cardiac Microenvironment." *Journal of Molecular and Cellular Cardiology* 42.2 (2007): 295-303. Web.

Lonergan, Thomas, Barry Bavister, and Carol Brenner. "Mitochondria in Stem Cells." *Mitochondrion* 7.5 (2007): 289-96. Web.

Muller-Borer, B., et al. "Calcium Dependent CAMTA1 in Adult Stem Cell Commitment to a Myocardial Lineage." *PloS one* 7.6 (2012): e38454. Web.

Murakami, T., et al. "Induction of Nuclear Respiratory Factor-1 Expression by an Acute Bout of Exercise in Rat Muscle." *Biochimica et biophysica acta* 1381.1 (1998): 113-22. Web.

Nesti, C., et al. "The Role of Mitochondria in Stem Cell Biology." *Bioscience reports* 27.1-3 (2007): 165-71. Web.

Piccoli, C., et al. "Characterization of Mitochondrial and Extra-Mitochondrial Oxygen Consuming Reactions in Human Hematopoietic Stem Cells. Novel Evidence of the

Occurrence of NAD(P)H Oxidase Activity." *The Journal of biological chemistry* 280.28 (2005): 26467-76. Web.

Pietila, M., et al. "Mitochondrial Function and Energy Metabolism in Umbilical Cord Blood- and Bone Marrow-Derived Mesenchymal Stem Cells." *Stem cells and development* 21.4 (2012): 575-88. Web.

Pietila, M., et al. "Mitochondrial Function Determines the Viability and Osteogenic Potency of Human Mesenchymal Stem Cells." *Tissue engineering.Part C, Methods* 16.3 (2010): 435-45. Web.

Pittenger, M. F., and B. J. Martin. "Mesenchymal Stem Cells and their Potential as Cardiac Therapeutics." *Circulation research* 95.1 (2004): 9-20. Web.

Spitkovsky, Dimitry, et al. "Activity of Complex III of the Mitochondrial Electron Transport Chain is Essential for Early Heart Muscle Cell Differentiation." *The FASEB Journal* (2004)Web.

Tormos, Kathryn V, et al. "Mitochondrial Complex III ROS Regulate Adipocyte Differentiation." *Cell Metabolism* 14.4 (2011): 537-44. Web.

Varum, S., et al. "Enhancement of Human Embryonic Stem Cell Pluripotency through Inhibition of the Mitochondrial Respiratory Chain." *Stem cell research* 3.2-3 (2009): 142-56. Web.

Virbasius, C. A., J. V. Virbasius, and R. C. Scarpulla. "NRF-1, an Activator Involved in Nuclear-Mitochondrial Interactions, Utilizes a New DNA-Binding Domain Conserved

in a Family of Developmental Regulators." *Genes & development* 7.12a (1993): 2431-45. Web.

Wade, M. H., J. E. Trosko, and M. Schindler. "A Fluorescence Photobleaching Assay of Gap Junction-Mediated Communication between Human Cells." *Science (New York, N.Y.)* 232.4749 (1986): 525-8. Web.

Xu, Meifeng, et al. "Differentiation of Bone Marrow Stromal Cells into the Cardiac Phenotype Requires Intercellular Communication with Myocytes." *Circulation* 110.17 (2004): 2658-65. Web.